Anderson transition on the Cayley tree as a traveling wave critical point for various probability distributions

2009 J. Phys. A: Math. Theor. 42 075002

(http://iopscience.iop.org/1751-8121/42/7/075002)

IOP PUBLISHING JOURNAL OF PHYSICS A: MATHEMATICAL AND THEORETICAL

J. Phys. A: Math. Theor. **42** (2009) 075002 (34pp) doi:10.1088/1751-8113/42/7/075002

Anderson transition on the Cayley tree as a traveling wave critical point for various probability distributions

Cécile Monthus and Thomas Garel

Institut de Physique Théorique, CNRS and CEA Saclay 91191 Gif-sur-Yvette Cedex, France

Received 12 November 2008
Published 21 January 2008
Online at stacks.iop.org/JPhysA/42/075002

Abstract

For Anderson localization on the Cayley tree, we study the statistics of various observables as a function of the disorder strength W and the number N of generations. We first consider the Landauer transmission T_N. In the localized phase, its logarithm follows the traveling wave form $\ln T_N \simeq \overline{\ln T_N} + \ln t^*$ where (i) the disorder-averaged value moves linearly $\overline{\ln(T_N)} \simeq -\frac{N}{\xi_{\rm loc}}$ and the localization length diverges as $\xi_{\rm loc} \sim (W - W_c)^{-\nu_{\rm loc}}$ with $\nu_{\rm loc} = 1$ and (ii) the variable t^* is a fixed random variable with a power-law tail $P^*(t^*) \sim 1/(t^*)^{1+\beta(W)}$ for large t^* with $0 < \beta(W) \leqslant 1/2$, so that all integer moments of T_N are governed by rare events. In the delocalized phase, the transmission T_N remains a finite random variable as $N \to \infty$, and we measure near criticality the essential singularity $\overline{\ln(T_\infty)} \sim -|W_c - W|^{-\kappa_T}$ with $\kappa_T \sim 0.25$. We then consider the statistical properties of normalized eigenstates $\sum_x |\psi(x)|^2 = 1$, in particular the entropy $S = -\sum_x |\psi(x)|^2 \ln |\psi(x)|^2$ and the inverse participation ratios (IPR) $I_q = \sum_x |\psi(x)|^{2q}$. In the localized phase, the typical entropy diverges as $S_{\rm typ} \sim (W - W_c)^{-\nu_S}$ with $\nu_S \sim 1.5$, whereas it grows linearly as $S_{\rm typ}(N) \sim N$ in the delocalized phase. Finally for the IPR, we explain how closely related variables propagate as traveling waves in the delocalized phase. In conclusion, both the localized phase and the delocalized phase are characterized by the traveling wave propagation of some probability distributions, and the Anderson localization/delocalization transition then corresponds to a traveling/non-traveling critical point. Moreover, our results point toward the existence of several length scales that diverge with different exponents ν at criticality.

PACS numbers: 71.23.An, 71.30.+h, 72.15.Rn

(Some figures in this article are in colour only in the electronic version)

1. Introduction

Since its discovery 50 years ago [1] Anderson localization has remained a very active field of research (see, for instance, the reviews [2–7]). According to the scaling theory [8], there is no delocalized phase in dimensions $d = 1, 2$, whereas there exists a localization/delocalization at finite disorder in dimension $d > 2$. To get some insight into this type of transition, it is natural to consider Anderson localization on the Cayley tree (or the Bethe lattice) which is expected to represent some mean-field limit. The tight-binding Anderson model on the Cayley tree has been thus studied by various authors. In [9], the recursion equation for the self-energy has been studied to establish the mobility edge as the limit of stability of localized states. In [10], the exponent ν governing the divergence of the localization length was shown to be $\nu = 1$. In [11], the supersymmetric formalism has been used to predict the critical behavior of some disorder-averaged observables (see also [12–15] where similar results have been obtained for the case where the Anderson tight-binding model is replaced by a nonlinear σ model).

In [16, 17], the problem was reformulated in terms of recursions on Riccati variables to obtain weak-disorder expansions. Other studies have focused on random-scattering models on the Cayley tree [18–20]. More recently, the interest in Anderson localization on the Cayley tree has been revived by the question of many-body localization [21], because the geometry of the Fock space of many-body states was argued to be similar to a Cayley tree [22–25]. In the present paper, we consider the Anderson tight binding model on the Cayley tree already studied in [9–11, 16, 17] and we study numerically the statistical properties of Landauer transmission and eigenstates as a function of the disorder strength W and of the number N of generations. We find that several probability distributions propagate as traveling waves with a fixed shape, as the number N of tree generations grows. The fact that traveling waves appear in disordered models defined on trees has been discovered by Derrida and Spohn [26] on the specific example of the directed polymer in a random medium and was then found in various models [27]. For the case of Anderson localization on trees, the analysis of [9] concerning the distribution of the self-energy in the localized phase is actually a 'traveling wave analysis' (see appendix A for more details), although it is not explicitly mentioned in these terms in [9]. The fact that traveling waves occur has been explicitly seen in the numerical study of the transmission distribution for a random-scattering model on the Cayley tree (see figure 8(*b*) of [20]) and has been found within the supersymmetric formalism [12, 14, 15]. In the field of traveling waves and front propagation (see the reviews [28, 29]), there exists an essential separation between two classes: in 'pulled fronts', the velocity is determined by the form of the tail of the front and thus by the appropriate linearized equation in the tail region, whereas in 'pushed fronts', the velocity is determined by the bulk properties and thus by the nonlinear dynamics in the bulk region. It turns out that for disordered systems defined on trees, the traveling waves that appear usually correspond to cases where it is the tail of the probability distribution that determines the velocity [26]. In particular for Anderson localization on the Cayley tree, the traveling wave propagation is also determined by the tails [9]. From this traveling wave point of view, the localization/delocalization Anderson transition thus represents a traveling/non-traveling critical point. Such a traveling/non-traveling phase transition for a branching random walk in the presence of a moving absorbing wall has been studied recently in [30] and we find here very similar behavior in the critical region.

The paper is organized as follows. In section 2, we describe the statistical properties of Landauer transmission. In section 3, we discuss the statistical properties of eigenstates, as measured by the entropy and inverse participation ratios (IPR). We summarize our conclusions in section 4. In appendix A, we translate the analysis of [9] concerning the distribution of the self-energy in the localized phase into a traveling-wave tail analysis for the Landauer

transmission discussed in section 2. In appendix B, we explain how such a similar tail analysis can be performed in the delocalized phase for auxiliary variables that are closely related to inverse participation ratios. Finally, in appendix C, we recall the results of [30] concerning the traveling/non-traveling phase transition for a branching random walk in the presence of a moving absorbing wall, since these results are used as a comparison in the text to understand the finite-size scaling properties in the critical region.

2. Statistical properties of the Landauer transmission

In quantum coherent problems, the most appropriate characterization of transport properties consists of defining a scattering problem where the disordered sample is linked to incoming wires and outgoing wires and of studying the reflection and transmission coefficients. This scattering theory definition of transport, first introduced by Landauer [31], has been much used for one-dimensional systems [32–34] and has been generalized to higher dimensionalities and multi-probes measurements (see the review [35]). In dimension $d = 1$, the transfer matrix formulation of the Schrödinger equation yields that the probability distribution of the Landauer transmission becomes asymptotically log-normal [32, 34] , i.e. one has

$$\ln T_L^{(1d)} = -\frac{L}{\xi_{\rm loc}} + L^{1/2} u \tag{1}$$

where $\xi_{\rm loc}$ represents the localization length and u is a sample-dependent random variable of order $O(1)$ distributed with a Gaussian law. Although it is often assumed that this log-normal distribution persists in the localized phase in dimensions $d = 2, 3$, recent numerical studies [36] are in favor of the following scaling form for the logarithm of the conductance:

$$\ln g_L^{(d)} = -\frac{L}{\xi_{\rm loc}} + L^{\omega(d)} u \tag{2}$$

with exponents of order $\omega(d = 2) \simeq 1/3$ and $\omega(d = 3) \simeq 1/5$ [36], whereas $\omega(d = 1) = 1/2$ from equation (1). For the Cayley tree that we consider in this paper, we will find below that the fluctuation exponent vanishes $\omega_{\rm Cayley} = 0$, and we will discuss the probability distribution of the variable u. But let us first recall the appropriate scattering framework for the Cayley tree [17] .

2.1. Reminder on the Miller–Derrida framework to compute the Landauer transmission [17]

We consider the Anderson tight-binding model

$$H = \sum_i \epsilon_i |i\rangle\langle i| + \sum_{\langle i,j\rangle} |i\rangle\langle j|, \tag{3}$$

where the hopping between nearest neighbors $\langle i, j\rangle$ is a constant $V = 1$ and where the on-site energies ϵ_i are independent random variables drawn from the flat distribution

$$p(\epsilon_i) = \frac{1}{W}\theta\left(-\frac{W}{2} \leqslant \epsilon_i \leqslant \frac{W}{2}\right). \tag{4}$$

The parameter W thus represents the disorder strength.

We consider the scattering geometry introduced in [17] and shown in figure 1: the finite tree of branching ratio K is attached to one incoming wire at its root (generation $n = 0$) and to K^{2N} outgoing wires at generation $2N$. One is interested in the eigenstate $|\psi\rangle$ that satisfies the Schrödinger equation

$$H|\psi\rangle = E|\psi\rangle \tag{5}$$

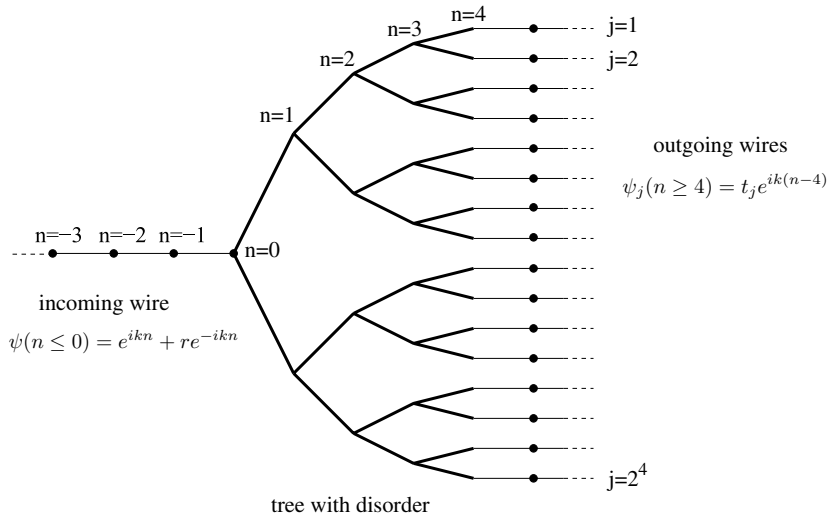

Figure 1. Scattering geometry of [17]: the disordered tree of branching ratio $K = 2$ starting at generation $n = 0$ and ending at generation $2N$ (on the figure $2N = 4$) is attached to one incoming wire and to K^{2N} outgoing wires. In section 2, we discuss the properties of the total transmission $T \equiv \sum_j |t_j|^2 = 1 - |r|^2$ where r is the reflection amplitude of the incoming wire, and t_j the transmission amplitudes of the outgoing wires.

inside the disorder sample and in the wires where one requires the plane-wave forms

$$\begin{aligned} \psi(n \leqslant 0) &= \mathrm{e}^{\mathrm{i}kn} + r\,\mathrm{e}^{-\mathrm{i}kn}, \\ \psi_j(n \geqslant 2N) &= t_j\,\mathrm{e}^{\mathrm{i}k(n-2N)}. \end{aligned} \tag{6}$$

These boundary conditions define the reflection amplitude r of the incoming wire and the transmission amplitudes t_j of the $j = 1, 2, \ldots, K^{2N}$ outgoing wires. To satisfy the Schrödinger equation of equation (5) within the wires with the forms of equation (6), one has the following relation between the energy E and the wave vector k:

$$E = 2\cos k. \tag{7}$$

To simplify the discussion, we will focus in this paper on the case of zero-energy $E = 0$ and wave vector $k = \pi/2$

$$\text{In this paper: } E = 0 \qquad \text{and} \qquad k = \pi/2 \tag{8}$$

because the zero-energy $E = 0$ corresponds to the center of the band where the delocalization first appears when the strength W of the disorder is decreased from the strong disorder localized phase.

Inside the Cayley tree $0 \leqslant n \leqslant 2N-1$, the Schrödinger equation of equation (5) involves one ancestor denoted by $\mathrm{anc}(n, j)$ and K descendants denoted by $\mathrm{des}_m(n, j)$

$$0 = \epsilon(n, j)\psi(n, j) + \psi(\mathrm{anc}(n, j)) + \sum_{m=1}^{K} \psi(\mathrm{des}_m(n, j)), \tag{9}$$

whereas for the last generation $2N$ there are only one ancestor and one descendant (outgoing wire)

$$0 = \epsilon(2N, j)\psi(2N, j) + \psi(\mathrm{anc}(2N, j)) + \psi(2N+1, j). \tag{10}$$

As explained in [17], it is convenient to introduce the Riccati variables

$$R(n, j) \equiv \frac{\psi(\mathrm{anc}(n, j))}{\psi(n, j)} \tag{11}$$

that represent the ratio of the wavefunction of two neighboring sites. On the outgoing wires, these Riccati variables are fixed by equation (6) to be

$$R(2N+1, j) = \frac{\psi(2N, j)}{\psi(2N+1, j)} = \mathrm{e}^{-\mathrm{i}k} = -\mathrm{i}. \tag{12}$$

The Schrödinger equation of equation (10) gives the first recursion

$$R(2N, j) = -\epsilon(2N, j) - \frac{1}{R(2N+1, j)} = -\epsilon(2N, j) - \mathrm{e}^{\mathrm{i}k} = -\epsilon(2N, j) - \mathrm{i}, \tag{13}$$

whereas the Schrödinger equation of equation (9) gives the recursion inside the tree for $0 \leqslant n \leqslant 2N-1$

$$R(n, j) = -\epsilon(n, j) - \sum_{m=1}^{K} \frac{1}{R(\mathrm{des}_m(n, j))}. \tag{14}$$

On the other hand, the value of the Riccati variable for the origin of the tree $n = 0$ is fixed by the incoming wire of equation (6)

$$R(0) = \frac{\psi(-1)}{\psi(0)} = \frac{\mathrm{e}^{-\mathrm{i}k} + r\,\mathrm{e}^{\mathrm{i}k}}{1+r} \tag{15}$$

and thus the reflection coefficient r can be obtained via

$$r = -\frac{R(0) - \mathrm{e}^{-\mathrm{i}k}}{R(0) - \mathrm{e}^{\mathrm{i}k}} = \frac{\mathrm{i} + R(0)}{\mathrm{i} - R(0)} \tag{16}$$

from the $R(0)$ obtained via the recursion of equation (14). From the conservation of energy, the total transmission T is related to the reflection coefficient $|r|^2$

$$T \equiv \sum_j |t_j|^2 = 1 - |r|^2. \tag{17}$$

As explained in [17], the criteria for the localization/delocalization phases are then the following:

(a) if the Riccati variable $R(0)$ at the root of the tree converges toward a real random variable as $N \to \infty$, the reflection is total $|r| = 1$ and the transmission vanishes $T = 0$.

(b) if the Riccati variable $R(0)$ keeps a finite negative imaginary part as $N \to \infty$, the reflection is only partial $|r| < 1$ and the transmission remains finite $T = 1 - |r|^2 > 0$.

We refer to [17] for the results of a weak disorder expansion within this framework, and for a numerical Monte Carlo approach to determine the mobility edge in the plane (E, W). Here we will instead study the statistical properties of the transmission T at zero energy $E = 0$ as a function of the disorder strength W (equation (4)) and of the number N of generations. But before discussing the disordered case, let us first describe the finite-size properties of the pure case.

2.2. *Example: transmission of finite pure trees*

In the pure case where all on-site energies vanish $\epsilon(n, j) = 0$, all branches are equivalent and there is no dependence on j. The recursions for Riccati variables of equations (12)–(14) give

$$\begin{aligned} &R_{\rm pure}(2N+1) = -{\rm i} \\ &R_{\rm pure}(2N) = -{\rm i} \\ &R_{\rm pure}(n) = -\frac{K}{R_{\rm pure}(n+1)} \qquad \text{for} \qquad 0 \leqslant n \leqslant 2N-1 \end{aligned} \tag{18}$$

i.e. one obtains the simple alternation between odd and even generations

$$\begin{aligned} &R_{\rm pure}(2N-1) = -\frac{K}{R_{\rm pure}(2N)} = -K{\rm i} \\ &R_{\rm pure}(2N-2) = -\frac{K}{R_{\rm pure}(2N-1)} = -{\rm i} \\ &\cdots \qquad\qquad\qquad \cdots \\ &R_{\rm pure}(1) = -K{\rm i} \end{aligned} \tag{19}$$

$$R_{\rm pure}(0) = -{\rm i}. \tag{20}$$

The reflection coefficient r thus vanishes exactly for any even size $(2N)$

$$r_{\rm pure} = \frac{{\rm i} + R_{\rm pure}(0)}{{\rm i} - R_{\rm pure}(0)} = 0 \tag{21}$$

and the transmission coefficient in each branch $j = 1, \ldots, K^{2N}$ reads

$$t_j^{\rm pure} = (1+r)\prod_{n=1}^{2N} \frac{1}{R_{\rm pure}(n)} = \frac{1}{(-K)^N}. \tag{22}$$

(Note that for pure trees of uneven size, the reflection would not vanish. This is why in the disordered case, we will only consider trees of even sizes $2N$ where in the corresponding pure case, the reflection vanishes exactly for any finite tree.) It is instructive to write now the corresponding wavefunction as a function of the generation n,

$$\begin{aligned} &\ldots \psi_{\rm pure}(-4) = 1 \\ &\psi_{\rm pure}(-3) = {\rm i} \\ &\psi_{\rm pure}(-2) = -1 \\ &\psi_{\rm pure}(-1) = -{\rm i} \\ &\psi_{\rm pure}(0) = 1 \\ &\psi_{\rm pure}(1) = \frac{\rm i}{K} \\ &\psi_{\rm pure}(2) = -\frac{1}{K} \\ &\psi_{\rm pure}(3) = -\frac{\rm i}{K^2} \\ &\psi_{\rm pure}(4) = \frac{1}{K^2} \ldots . \end{aligned} \tag{23}$$

This exponential decay of the wavefunction in this delocalized case is very peculiar to the tree geometry: it is imposed by the energy conservation and by the exponential growth of the number of sites with the generation n.

2.3. Statistics over the disordered samples of the transmission T_N

2.3.1. Numerical pool method. If one wishes to study numerically real trees, one is limited to rather small number of generations of order $N_{\max} \sim 12, 14$ (see, for instance, the study [37] based on exact diagonalization) because the number of sites and thus of random energies grows exponentially in N. From the point of view of convergence toward stable probability distributions via recursion relations, it is thus better to use the so-called pool method that will allow us to study much larger number of generations (see equation (27)). The idea of the pool method is the following: at each generation, one keeps the same number $M_{\rm pool}$ of random variables to represent probability distributions. Within our present framework, the probability distribution $P_n(R)$ of the Riccati variables R at generation n will be represented by a pool of $M_{\rm pool}$ complex values $\left\{R_n^{(1)}, \ldots, R_n^{(M_{\rm pool})}\right\}$. It is convenient from now on to change the notation $n \to 2N - n$ with respect to figure 1 so that $n = 0$ now corresponds to the contacts with the outgoing wires (see figure 1). The numerical results presented below have been obtained with the following procedure:

(i) the random variables of the initial pool are given by (equation (13))

$$R_0(j) = -\epsilon_0(j) - \mathrm{i}, \tag{24}$$

where $\epsilon(j)$ are independent random variables drawn with equation (4).

(ii) From the random variables $R_{n-1}(j)$ of the pool at generation $n-1$, the pool at generation n is constructed as follows. For each $j = 1, 2, \ldots, M_{\rm pool}$, one generates a new random energy $\epsilon_n(j)$ with the law of equation (4) and one draws K random indices $\{j_1(j), \ldots, j_K(j)\}$ among the pool of generation $(n-1)$ to construct the variable $R_n(j)$ as follows (equation (14)):

$$R_n(j) = -\epsilon_n(j) - \sum_{m=1}^{K} \frac{1}{R_{n-1}(j_m(j))}. \tag{25}$$

(iii) From these pools of Riccati variables, one may compute via equations (16) and (17) a pool of total transmission $T_n(j)$ for trees of n generations using

$$T_n(j) = 1 - |r_n(j)|^2 = 1 - \left|\frac{\mathrm{i} + R_n(j)}{\mathrm{i} - R_n(j)}\right|^2. \tag{26}$$

For the Anderson model on the Bethe lattice, the pool method has been already used, in particular in [9] with a pool $M_{\rm pool} = 1800$ with a number $N_{\max} \sim 30$ of generations, in [17] with pools up to $M_{\rm pool} = 10000$, and in [20] with pools up to $M_{\rm pool} = 16384$ with a number $N_{\max} \sim 400$ of generations. The pool method is also very much used for disordered systems on hierarchical lattices (see, for instance, [38–40]).

In the remainder of this section, we present the numerical results obtained with a pool of size

$$M_{\rm pool} = 10^5 \text{ with a number of generations } N \leqslant N_{\max} = 34.10^5. \tag{27}$$

We have also results for a pool of size $M_{\rm pool} = 10^6$ with a number of generations $N \leqslant N_{\max} = 24.10^4$ to see how the results change with the pool size. However, the number of generations N_g for this bigger pool $M_{\rm pool} = 10^6$ has turned out to lead to be less precise in the critical region. All figures shown below thus correspond to data obtained with the pool of size $M_{\rm pool} = 10^5$.

As is usual with the pool method [40], the location of the critical point depends on the pool, i.e. on the discrete sampling with $M_{\rm pool}$ values of probability distributions. It is expected to converge toward the thermodynamic critical point only in the limit $M_{\rm pool} \to \infty$

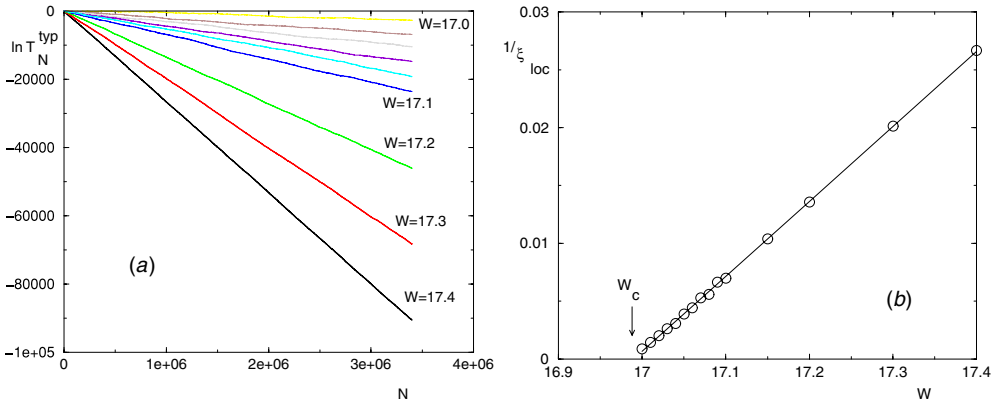

Figure 2. Exponential decay of the typical transmission $T_N^{\rm typ} \equiv e^{\overline{\ln T_N}}$ in the localized phase $W > W_c$: (*a*) linear decay of $\overline{\ln T_N}$ as a function of the number N of generations (see equation (30)). (*b*) Behavior of the slope $1/\xi_{\rm loc}(W)$ as a function of the disorder strength W: it vanishes linearly $1/\xi_{\rm loc}(W) \sim (W - W_c^{\rm pool})^{\nu_{\rm loc}}$ with $W_c^{\rm pool} \simeq 16.99$ (see equation (28)) and $\nu_{\rm loc} = 1$ (see equation (31)).

(see the discussion of appendix B.3). Nevertheless, for each given pool, the critical behavior with respect to this pool-dependent critical point usually allows a good measure of critical exponents [40]. For instance, for the pool of size $M_{\rm pool} = 10^5$, the critical value W_c of the disorder strength where the localization–delocalization occurs for the Landauer transmission is of order

$$W_c(M_{\rm pool} = 10^5) \simeq 16.99. \tag{28}$$

For the pool of size $M_{\rm pool} = 10^6$, we find that it is higher and of order $W_c(M_{\rm pool} = 10^6) \simeq 17.32\ldots$. This rather important shift of the pseudo-critical point with the pool size which has already been seen in [17], seems to be due to the very slow logarithmic convergence of traveling wave velocity in the presence of cut-off (see the discussion of appendix B.3). So we stress that here, in contrast to [9, 17], our goal is not to determine the true thermodynamic mobility edge $W_c(+\infty)$, but instead to understand the critical behavior of the finite-pool results with respect to the pool-dependent critical point of equation (28).

We will first discuss the behavior of the typical transmission $T_N^{\rm typ}$ defined by

$$\ln\left(T_N^{\rm typ}\right) \equiv \overline{\ln T_N}, \tag{29}$$

as a function of the number N of generations and disorder strength W, before we turn to the distribution around this typical value.

2.3.2. Exponential decay of the typical transmission $T_N^{\rm typ}$ in the localized phase $W > W_c$. In the localized phase, one expects that the typical transmission $T_N^{\rm typ}$ defined by equation (29) decays exponentially with the number N of generations

$$\ln\left(T_N^{\rm typ}\right) \equiv \overline{\ln T_N(W > W_c)} \underset{N\to\infty}{\simeq} -\frac{N}{\xi_{\rm loc}(W)} \tag{30}$$

where $\xi_{\rm loc}$ represents the localization length that diverges at the delocalization transition

$$\xi_{\rm loc}(W) \underset{W\to W_c^+}{\simeq} (W - W_c)^{-\nu_{\rm loc}}. \tag{31}$$

We show in figure 2 our numerical results for the pool of size $M_{\rm pool} = 10^5$ (equation (27)): the exponential decay with N of equation (30) is shown in figure 2(*a*) for various disorder

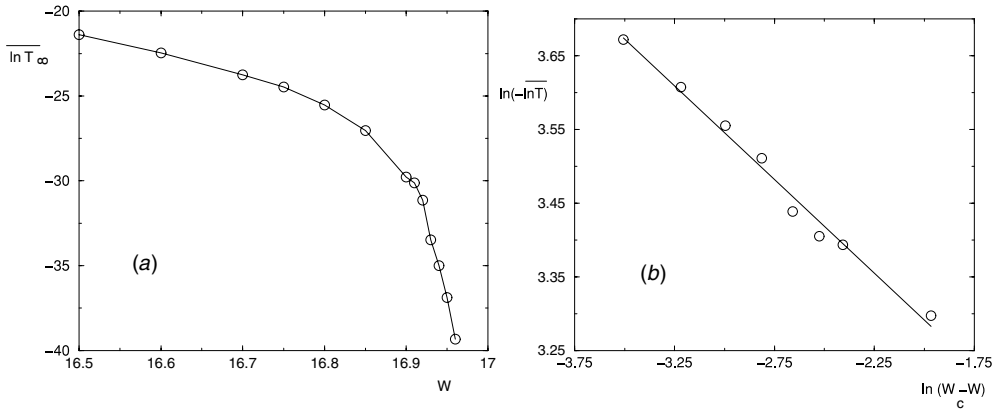

Figure 3. Behavior of the typical transmission $T_\infty^{\rm typ}$ of the infinite tree in the delocalized phase: (a) $\ln T_\infty^{\rm typ} \equiv \overline{\ln T_\infty(W < W_{\rm c})}$ as a function of the disorder strength W, (b) same data in a log–log plot to measure the exponent of the essential singularity of equation (34): $\ln(-\ln T_\infty^{\rm typ})$ as a function of $\ln(W_{\rm c} - W)$: the slope is of order $\kappa_T \sim 0.25$.

strengths W. The corresponding slope $1/\xi_{\rm loc}(W)$ is shown as a function of W in figure 2(b): we find that this slope vanishes linearly in $(W - W_{\rm c})$, in agreement with the exact result [10, 11]

$$\nu_{\rm loc} = 1 \tag{32}$$

and in agreement with figure 7 of [20] concerning a random-scattering model on the Cayley tree.

2.3.3. Behavior of the typical transmission $T_\infty^{\rm typ}$ in the delocalized phase $W < W_{\rm c}$ near criticality.

In the delocalized phase, the typical transmission remains finite in the limit where the number of generations N diverges

$$\overline{\ln T_N(W < W_{\rm c}, N)} \underset{N\to\infty}{\simeq} \overline{\ln T_\infty(W < W_{\rm c})} > -\infty. \tag{33}$$

As shown in figure 3, we measure the following essential singularity behavior of the typical transmission:

$$\overline{\ln T_\infty(W < W_{\rm c})} \underset{W\to W_{\rm c}^-}{\simeq} -(W_{\rm c} - W)^{-\kappa_T} \qquad \text{with} \qquad \kappa_T \sim 0.25. \tag{34}$$

The presence of essential singularities in transport properties near the localization transition on the Bethe lattice has been found in [11] via the supersymmetric formalism (see also [12–15] where similar results have been obtained for the case where the Anderson tight-binding model is replaced by a nonlinear σ model). In particular, equation (71) of [11]) states that the leading critical behavior of the diffusion constant is given by: $\ln \mathcal{D} \sim -|E - E_{\rm c}|^{-1/2}$ (equation (71) of [11]). We note that the exponent in this essential singularity is $1/2$ instead of the exponent of order $1/4$ that we measure. The reason for this difference could be that the results of [11] are based on the computation of the *disorder-averaged two-point density–density correlation function* (see equation (2) of [11]), whereas our numerical results concern the *typical value of Landauer transmission*, and not the disorder-averaged transmission which is expected to be governed by rare events (see section 2.3.5). Also it is not clear to us what exactly represents the

diffusion constant computed in [11], because it is known that on the Bethe lattice the dynamics is not diffusive but ballistic in the delocalized phase [41], and that more generally the random walk on the Bethe lattice is not diffusive because the tree geometry induces an effective bias away from the origin (see, for instance, [42] and references therein). As a consequence, some implicit reinterpretation of the Bethe lattice seems to underlie the statements of [11] that makes difficult a precise comparison with our present numerical results.

2.3.4. Finite-size scaling in the critical region. If there exists some finite-size scaling in the critical region for the typical Landauer transmission of the form

$$\overline{\ln T_N(W)} \simeq -N^{\rho_T} G(N^{1/\nu_T^{\rm FS}}(W_{\rm c}-W)) \tag{35}$$

the matching of our results in the localized phase (see equation (30)) and in the delocalized phase (equation (34)) requires a finite-size correlation length exponent $\nu_T^{\rm FS}$ of order

$$\nu_T^{\rm FS} = \nu_{\rm loc} + \kappa_T = 1 + \kappa_T \simeq 1.25. \tag{36}$$

In another traveling/non-traveling phase transition studied in [30] (see the summary in appendix C), it has been obtained that the finite-size scaling exponent $\nu_{\rm FS}$ is determined by the relaxation rate toward the finite value in the non-traveling phase. We have thus studied the relaxation length toward the finite value in the delocalized phase. We find that our data for $\ln T_N$ are compatible with the form

$$\overline{\ln T_N(W < W_{\rm c})} \simeq -(W_{\rm c}-W)^{-\kappa_T} a_N, \tag{37}$$

where a_N is a random stationary process as a function of N. We find that its autocorrelation function is exponential

$$C(N) \simeq {\rm e}^{-\frac{N}{\xi_{\rm relax}(W)}} \tag{38}$$

and we measure that the relaxation length $\xi_{\rm relax}(W)$ diverges with an exponent

$$\xi_{\rm relax}(W) \propto \frac{1}{(W_{\rm c}-W)^{\nu_{\rm relax}}} \qquad \text{with} \qquad \nu_{\rm relax} \simeq 1.21 \tag{39}$$

of the order of the exponent $\nu_T^{\rm FS}$ of equation (36). We thus obtain that the critical properties are qualitatively similar to the critical properties described in [30] (see the summary in appendix C): the traveling phase is characterized by a velocity that vanishes linearly, but the finite size scaling is governed by the relaxation length toward the asymptotic finite value of the non-traveling phase. Exactly at criticality, we thus expect the following stretched exponential decay of the typical transmission:

$$\overline{\ln T_N(W_{\rm c})} \simeq -N^{\rho_T}, \tag{40}$$

where the exponent ρ_T is related to the other exponents by (see the scaling relations of equations (C.9) and (C.11) in appendix C)

$$\rho_T = \frac{\kappa_T}{\nu_T^{\rm FS}} = 1 - \frac{1}{\nu_T^{\rm FS}}. \tag{41}$$

From our previous estimate of the exponent $\kappa_T \simeq 0.25$, this would correspond to the numerical value

$$\rho_T = \frac{\kappa_T}{1+\kappa_T} \simeq 0.2. \tag{42}$$

We have not been able to measure this stretched exponential behavior exactly at criticality from our data, because a precise measure of the exponent ρ_T would require to be exactly at the critical point.

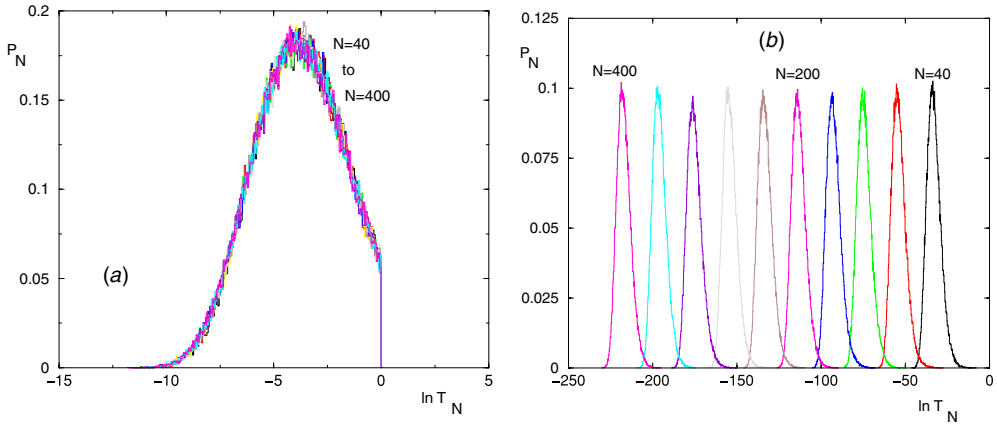

Figure 4. Evolution with N of the probability distribution $P_N(\ln T_N)$ of the logarithm of Landauer transmission: (a) in the delocalized phase (here $W = 10$), the probability distribution $P_N(\ln T_N)$ does not move with N, and vanishes with a discontinuity at the boundary $\ln T_N = 0$. (b) In the localized phase (here $W = 25$), the probability distribution $P_N(\ln T_N)$ moves with N as a traveling wave of fixed shape.

2.3.5. Distribution of the logarithm of the transmission. Up to now, we have only discussed the behavior of the typical transmission of equation (29) as a function of N and W. We now turn to the probability distribution of the logarithm of the transmission around its averaged value, i.e. we consider the distribution of the relative variable

$$u \equiv \ln T_N - \overline{\ln T_N}. \tag{43}$$

We find that as $N \to \infty$, this variable remains finite not only in the delocalized phase where $\overline{\ln T_\infty}$ is finite, but also in the localized phase where $\overline{\ln T_N}$ decays linearly in N (equation (30)). This means that in the localized phase, the probability distributions $P_N(\ln T_N)$ actually propagate as a traveling wave with a fixed shape around its moving center $\overline{\ln T_N}$ as shown in figure 4(b). This phenomenon has already been seen for random scattering models on the Bethe lattice (see figure 8(b) of [20]). This is in contrast to the broadening with L observed in low dimensions $d = 1, 2, 3$ (see equation (2)): the Cayley tree thus corresponds to $\omega_{\text{Cayley}} = 0$ in equation (2).

The fact that the shape is fixed can be used numerically to measure more precisely the tails of this probability distribution by accumulating data over iterations: we show in figure 5(a) the histograms of u obtained by this procedure for various disorder strengths W. An essential property of this distribution is the right exponential tail

$$P_W(u) \underset{u\to+\infty}{\simeq} \mathrm{e}^{-\beta(W)u}. \tag{44}$$

In terms of the rescaled transmission $t = T_N / T_N^{\text{typ}} = \mathrm{e}^u$ (see equation (43)), this corresponds to the power-law decay

$$P\left(t = T_N / T_N^{\text{typ}}\right) \underset{t\to+\infty}{\simeq} \frac{1}{t^{1+\beta(W)}}. \tag{45}$$

We find that the selected exponent $\beta_{\text{selec}}(W)$ slightly grows as the disorder strength W decreases, from a value of order $\beta(W = 100) \simeq 0.33$ for the strong disorder $W = 100$ toward a value of order $\beta(W = 17) \simeq 0.48$ near criticality (see figure 5(a)). The velocity of the traveling wave propagation of the whole distribution is actually determined by this power-law

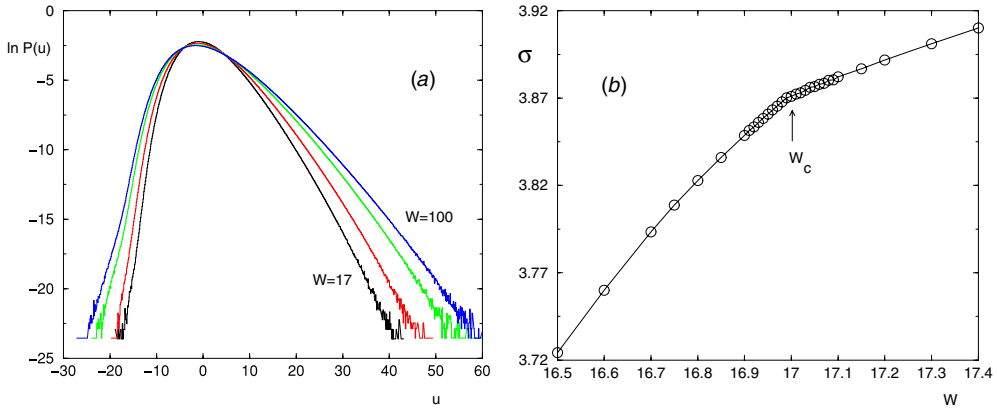

Figure 5. (*a*) Logarithm of the probability distribution $P(u)$ of $u = \ln T_N - \overline{\ln T_N}$ as W varies in the localized phase for various disorder strengths $W = 17, 25, 50, 100$: the exponential decay as $e^{-\beta u}$ corresponds to slopes of order $\beta(W = 17) \simeq 0.48, \beta(W = 25) \simeq 0.43, \beta(W = 50) \simeq 0.35, \beta(W = 100) \simeq 0.33$. (*b*) Width $\sigma = (\overline{u^2})^{1/2}$ of the probability distribution of $u = \ln T_N - \overline{\ln T_N}$ as a function of W: it remains finite both in the localized phase and in the delocalized phase, but it presents a cusp singularity at criticality.

tail, as explained in detail in appendix A. In particular, the critical value $\beta(W \to W_c) = 1/2$ has been predicted in [9] (see equation (A.33) in appendix A). An important consequence of the power-law tail of equation (45) with $\beta(W) \leqslant 1/2$ is that all integer moments $\overline{T_N^n}$ of the Landauer transmission will be governed by rare events.

Finally, we show in figure 5(*b*) the width of the probability distribution of $\ln T_N$ as a function of W: it remains finite both in the localized phase and in the delocalized phase, but it presents a cusp singularity at criticality because in the delocalized phase, the distribution presents a singularity at finite distance from the typical value, as is clearly visible in figure 4(*a*): the transmission is bounded by $T \leqslant 1$, i.e. the histogram of $\ln T_N$ presents a discontinuity at $\ln T_N = 0$.

3. Statistics of eigenstates

The Landauer transmission studied in the previous section is of course the most appropriate observable to characterize the transport properties and to find the transition between the conducting/non-conducting phases. However, one expects that these transmission properties that emerge when the disordered sample is linked to incoming and outgoing wires are related to the nature of eigenstates of the disordered sample in the absence of these external wires (see figure 6). To determine whether a normalized eigenstate

$$\sum_x |\psi(x)|^2 = 1 \tag{46}$$

is localized or delocalized, the usual parameters are the inverse participation ratios

$$I_q \equiv \sum_x |\psi(x)|^{2q} \tag{47}$$

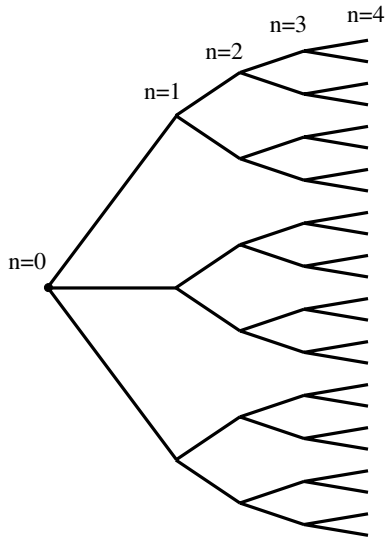

Figure 6. Cayley tree with branching ratio $K = 2$ where each interior site has $K+1 = 3$ neighbors. In the figure the tree ends at generation $2N = 4$.

of arbitrary power q. Another important quantity to characterize the spatial extent of an eigenstate is its entropy

$$S \equiv -\sum_x |\psi(x)|^2 \ln |\psi(x)|^2. \tag{48}$$

The normalization condition yields the identity $I_{q=1} = 1$, and the entropy corresponds to

$$S = -\partial_q I_q|_{q=1} = -\partial_q \ln I_q|_{q=1}. \tag{49}$$

On a hypercubic lattice of size L in dimension d, containing $\mathcal{N}_L = L^d$ sites, the delocalized phase is characterized by the following typical behavior:

$$\overline{\ln I_q} \sim -d(q-1)\ln L = -(q-1)\ln \mathcal{N}_L. \tag{50}$$

and

$$\overline{S} \sim d \ln L = \ln \mathcal{N}_L \tag{51}$$

These scalings are the same for pure homogeneous eigenfunctions with $|\psi(x)| = 1/L^d$ for all sites $x \in L^d$. At criticality, the scalings of the IPR involve a whole series of non-trivial exponents and the wavefunction is said to be multifractal (see the review [7]). Finally in the localized phase, the IPR and the entropy are finite.

In the present section, we discuss the statistical properties of these IPR and entropy for zero-energy eigenstates for the Cayley tree of figure 6 as a function of the number N of tree generations and of the disorder strength W.

3.1. Reminder on the Miller–Derrida framework to construct eigenstates

We refer to [17] where it is explained how eigenstates of finite trees can be constructed and how the density of states can be obtained. Note that on a tree, boundary sites dominate so that one needs a subtraction procedure to obtain the appropriate bulk density of states. In the following,

we are not interested in the density of states, which does not contain any information on the localized/delocalized nature of the spectrum. We wish to study instead the spatial properties of eigenstates of zero-energy $E = 0$ (center of the band). The Schrödinger equation (9) yields as before the recursion of equation (14) for the Riccati variables defined in equation (11). The difference with the scattering case is now in the boundary conditions

$$R(2N, j) = -\epsilon(2N, j) \tag{52}$$

that replace equation (13). As a consequence, the Riccati variables are now real (and not complex). The energy $E = 0$ will indeed be an eigenstate only if the Schrödinger equation is also satisfied at the center of the finite tree at the center site

$$0 = \epsilon(0) + \sum_{m=1}^{K+1} \frac{1}{R(\mathrm{des}_m(0))}. \tag{53}$$

Since the on-site energy $\epsilon(0)$ is a random variable drawn with some distribution, we may consider that we choose $\epsilon(0)$ to satisfy equation (53) to obtain a typical eigenstate of zero energy and to study its spatial properties. Let us first describe zero-energy eigenstate in the pure case to stress the peculiarities of the tree geometry.

3.2. Structure of zero-energy eigenstate on the pure tree

In the pure case where all on-site energies vanish $\epsilon(n, j) = 0$, the zero-energy eigenstate with radial symmetry reads

$$\psi_{2n-1} = 0, \tag{54}$$

$$\psi_{2n} = \psi_0 \left(-\frac{1}{K}\right)^n, \tag{55}$$

where the root amplitude ψ_0 is determined by the normalization condition

$$1 = \sum_x |\psi(x)|^2 = |\psi_0|^2 + (K+1)K|\psi_2|^2 + (K+1)K^3|\psi_4|^2 + \cdots + (K+1)K^{2N-1}|\psi_{2N}|^2$$

$$= |\psi_0|^2 \left[1 + \frac{K+1}{K} N\right]. \tag{56}$$

This state is the analog of the scattering state described in section 2.2. In particular, one sees again an exponential decay of the wavefunction in this delocalized case which is very peculiar to the tree geometry: in the normalization condition of equation (56), this exponential decay is exactly compensated by the exponential growth of the number of sites at generation $2n$, so that all generations $2n = 2, 4, \ldots, 2N$ carry exactly the same weight in the normalization condition, and the root weight $|\psi_0|^2$ vanishes as $1/N$ in the thermodynamic limit, where $(2N)$ is the number of generations of the tree.

For this state, the usual inverse participation ratio of equation (47) for $q = 2$ reads

$$I_2^{\mathrm{pur}}(2N) = \sum_x |\psi(x)|^4 = |\psi_0|^4 + (K+1)K|\psi_2|^4$$

$$+ (K+1)K^3|\psi_4|^4 + \cdots + (K+1)K^{2N-1}|\psi_{2N}|^4 \tag{57}$$

$$= |\psi_0|^4 \left[1 + \frac{K+1}{K^3} \frac{1 - \left(\frac{1}{K^2}\right)^N}{1 - \frac{1}{K^2}}\right]. \tag{58}$$

More generally for $q > 1$, one obtains the following decay with the number of generations

$$I_q^{\mathrm{pur}}(2N) \underset{N\to\infty}{\propto} |\psi_0|^{2q} \sim \frac{1}{N^q} \qquad \text{for} \qquad q > 1 \tag{59}$$

In terms of the total number of sites

$$\mathcal{N}(2N) = 1 + (K+1)\sum_{n=1}^{2N-1} K^n = 1 + (K+1)\frac{K^{2N}-1}{K-1} = \frac{K^{2N}(K+1)-2}{K-1} \tag{60}$$

this corresponds to

$$\ln I_q^{\rm pur}(2N) \underset{N\to\infty}{\propto} -q \ln N \underset{N\to\infty}{\propto} -q \ln(\ln \mathcal{N}(2N)) \qquad \text{for} \qquad q > 1. \tag{61}$$

This behavior is thus very anomalous with respect to the corresponding decay as $(-(q-1)\ln \mathcal{N}_L)$ for the IPR of pure states in finite dimension d (see equation (50)).

Moreover, since the eigenfunction normalization yields the identity $I_{q=1} = 1$, one sees that there exists some discontinuity as $q \to 1$. In particular, the entropy of equation (48) which can usually be computed as the derivative of equation (49) should be computed directly here, and one obtains

$$\begin{aligned} S^{\rm pur}(2N) &= -|\psi(0)|^2 \ln|\psi(0)|^2 - (K+1)K|\psi(2)|^2 \ln|\psi(2)|^2 \\ &\quad - \cdots - (K+1)K^{2N-1}|\psi(2N)|^2 \ln|\psi(2N)|^2 \qquad (62) \\ &= |\psi(0)|^2 \left[-\left(1 + \frac{K+1}{K}N\right) \ln|\psi(0)|^2 + \frac{K+1}{K} N(N+1)\ln K \right]. \qquad (63) \end{aligned}$$

Using equation (56), one obtains the following behavior for large N:

$$S^{\rm pur}(2N) = \ln\left(1 + \frac{K+1}{K}N\right) + \frac{\frac{K+1}{K}N(N+1)\ln K}{\left(1+\frac{K+1}{K}N\right)} \underset{N\to\infty}{\simeq} N \ln K. \tag{64}$$

In terms of the total number of sites of equation (60), the entropy is proportional to the logarithm of the number of sites

$$S^{\rm pur}(2N) \underset{N\to\infty}{\simeq} N \ln K \underset{N\to\infty}{\simeq} \tfrac{1}{2} \ln \mathcal{N}(2N) \tag{65}$$

that should be compared with the growth as $\ln \mathcal{N}(2N)$ for pure eigenstates in dimension d (see equation (51)).

In conclusion, the tree geometry induces very anomalous scalings in $(\ln\ln \mathcal{N})$ for the logarithm of IPR of pure states (see equation (61)) with respect to the case of finite dimension d, whereas the entropy is well behaved in $(\ln \mathcal{N})$ (see equation (65)). In the disordered case, we expect to observe similar behavior, whereas the IPR and the entropy will remain finite in the localized phase.

3.3. Recursion relation for inverse participation ratios

To compute the inverse participation ratio I_q (equation (47)) via recursion, one needs to introduce besides the Riccati variable of equation (11) the auxiliary variables defined by

$$C^{(q)}(n,j) = \left|\frac{\psi(n,j)}{\psi(\mathrm{anc}(n,j))}\right|^{2q} + \sum_l \left|\frac{\psi(l)}{\psi(\mathrm{anc}(n,j))}\right|^{2q}, \tag{66}$$

where the sum is over all sites l that are descendants of the site (n,j) of the tree. These variables satisfy the following recurrence inside the tree $1 \leqslant n \leqslant 2N-1$:

$$C^{(q)}(n,j) = \left(\frac{1}{R^2(n,j)}\right)^q \left[1 + \sum_{m=1}^{K} C^{(q)}(\mathrm{des}_m(n,j))\right] \tag{67}$$

and the initial conditions at the boundaries

$$C^{(q)}(2N,j) = \left(\frac{1}{R^2(2N,j)}\right)^q. \tag{68}$$

At the central root, one needs to impose the normalization

$$1 = \sum_x |\psi(x)|^2 = |\psi(0)|^2 \left[1 + \sum_{m=1}^{K+1} C^{(1)}(1,m) \right] \tag{69}$$

that determines the weight $|\psi(0)|^2$ of the root in terms of the variables $C^{(1)}$ of the branches.

To compute the inverse participation ratio of parameter q of equation (47), one needs the variables $C^{(q)}$ together with the variables $C^{(1)}$

$$I_q = \sum_x |\psi(x)|^{2q} = |\psi(0)|^{2q} \left[1 + \sum_{m=1}^{K+1} C^{(q)}(1,m) \right] = \frac{\left[1 + \sum_{m=1}^{K+1} C^{(q)}(1,m) \right]}{\left[1 + \sum_{m=1}^{K+1} C^{(1)}(1,m) \right]^q}. \tag{70}$$

3.4. Recursion for the entropy

To compute recursively the entropy of equation (48), one needs similarly to introduce the auxiliary variable

$$\sigma(n,j) = -\sum_l \frac{|\psi_l|^2}{\sum_{l'} |\psi_{l'}|^2} \ln \frac{|\psi_l|^2}{\sum_{l'} |\psi_{l'}|^2}, \tag{71}$$

where the sum over l denotes the sum over the site (n,j) and all its descendants: $\sigma(n,j)$ thus represents the entropy for the branch containing (n,j) and its descendants.

The initial conditions at the boundaries are simply

$$\sigma(2N,j) = 0 \tag{72}$$

and the recursion inside the tree $1 \leqslant n \leqslant 2N-1$ can be written as

$$\sigma(n,j) = \frac{\sum_{m=1}^{K} C^{(1)}(\mathrm{des}_m(n,j)) \sigma(\mathrm{des}_m(n,j))}{1 + \sum_{m=1}^{K} C^{(1)}(\mathrm{des}_m(n,j))} + S_{\mathrm{mix}}, \tag{73}$$

where the first term represents the weighted contribution of the branches entropies and where the second term represents the mixing entropy

$$S_{\mathrm{mix}} = -p_0 \ln p_0 - \sum_{m'=1}^{K} p_{m'} \ln p_{m'} \tag{74}$$

with the weights

$$p_0 = \frac{1}{\left(1 + \sum_{m=1}^{K} C^{(1)}(\mathrm{des}_m(n,j))\right)} \tag{75}$$

$$p_{m'} = \frac{C^{(1)}(\mathrm{des}_{m'}(n,j)))}{\left(1 + \sum_{m=1}^{K} C^{(1)}(\mathrm{des}_m(n,j))\right)} \tag{76}$$

normalized to $p_0 + \sum_{m'=1}^{K} p_{m'} = 1$. At the central site of the tree, one uses the same formula but with $(K+1)$ branches instead of K branches.

3.5. Numerical results on the statistics of eigenstates

3.5.1. Numerical pool method. To study the statistical properties of eigenstates, we have used again the pool method explained in section 2.3.1. The only difference is that for the transmission, we have followed the recursions for the complex Riccati variables, whereas here we follow the recursions for the real Riccati variable R and for the auxiliary variables $C^{(1)}$, $C^{(2)}$ and σ described above.

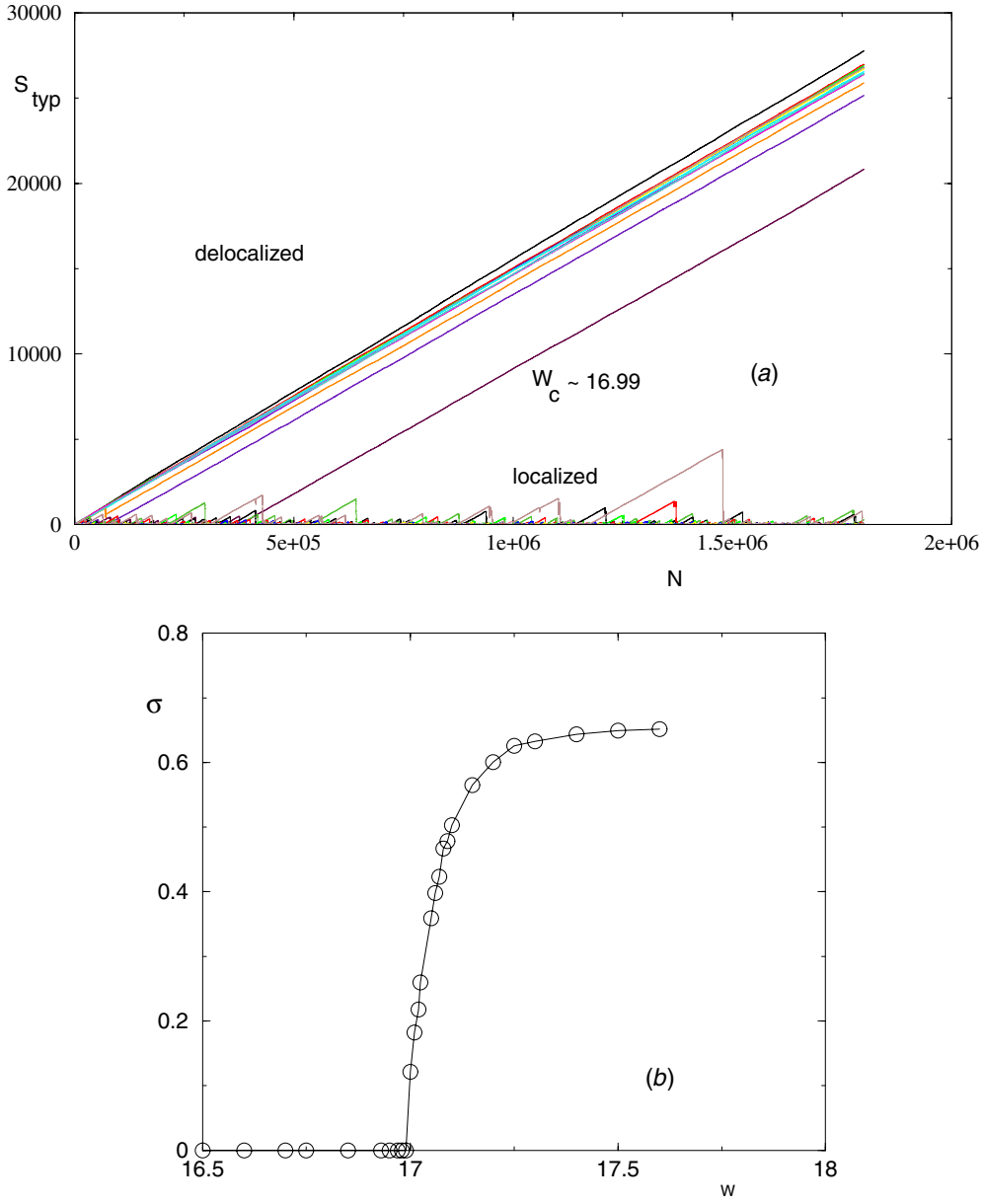

Figure 7. Statistics of the entropy $S(N) \equiv -\sum_x |\psi(x)|^2 \ln |\psi(x)|^2$ of a normalized zero-energy eigenstate: (a) evolution of the typical entropy $S_{\rm typ}(N) \equiv e^{\overline{\ln S(N)}}$ with the number N of generations: it grows linearly in N in the delocalized phase, whereas it remains finite in the localized phase. (b) Asymptotic width $\sigma = (\overline{v^2})^{1/2}$ of the relative variable $v = \ln S - \overline{\ln S}$ as a function of the disorder strength W: the width converges to 0 (as $1/N$) in the delocalized phase, whereas it is finite in the localized phase.

3.5.2. Statistics of the entropy of an eigenstate. We first consider how the eigenstate entropy defined in equation (48) evolves with the number N of generations. As shown in figure 7(a), the typical value grows linearly in N in the delocalized phase

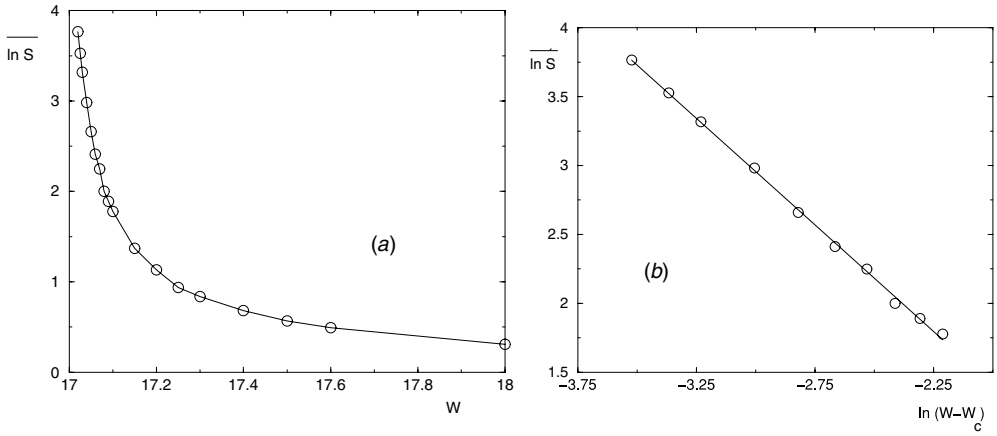

Figure 8. Critical behavior of the typical entropy $S_{\rm typ}(N=\infty) = e^{\overline{\ln S(N=\infty)}}$ in the localized phase (*a*) $\ln S_{\rm typ}(N=\infty) = \overline{\ln S(N=\infty)}$ as a function of the disorder strength W near the critical point. (*b*) The same data as a function of $\ln(W - W_c)$ to measure the exponent of the power law of equation (79): the slope is of order $\nu_S \simeq 1.5$.

$$S_{\rm typ}(N, W < W_c) \equiv e^{\overline{\ln S(N)}} \underset{N\to\infty}{\simeq} aN \tag{77}$$

where the factor a varies smoothly with W and does not vanish continuously near the critical point. In this delocalized phase, we moreover find that the width of the relative variable $v = \ln S_N - \overline{\ln S_N}$ decays to zero as $N \to \infty$

$$[\overline{(\ln S_N - \overline{\ln S_N})^2}]^{1/2}_{W<W_c} \underset{N\to\infty}{\simeq} \frac{1}{N}. \tag{78}$$

In the localized phase in contrast, the typical value and the width of the relative variable $v = \ln S_N - \overline{\ln S_N}$ remain finite as $N \to +\infty$ (see figures 7(*a*) and (*b*)).

As shown in figure 8, we find that the typical entropy of an infinite tree of the localized phase diverges with the following power law near criticality:

$$S_{\rm typ} \equiv e^{\overline{\ln S(N=+\infty)}} \underset{W\to W_c^+}{\simeq} \frac{1}{(W - W_c)^{\nu_S}} \qquad \text{with} \qquad \nu_S \simeq 1.5. \tag{79}$$

The entropy measures the size of the region where the weight $|\psi(x)|^2$ is concentrated, whereas the localization length $\xi_{\rm loc} \sim 1/(W - W_c)^{\nu_{\rm loc}=1}$ describes the far exponential decay of the transmission T (equation (30)). We thus conclude that in the localized phase, besides the localization length $\xi_{\rm loc} \sim 1/(W - W_c)^{\nu_{\rm loc}=1}$ known since [10], there exists a larger diverging length scale

$$\xi_S(W > W_c) \underset{W\to W_c^+}{\propto} \frac{1}{(W - W_c)^{\nu_s \sim 1.5}} \tag{80}$$

that characterizes the size where the weight $|\psi(x)|^2$ is concentrated.

3.5.3. Statistics of the root weight $|\psi_N(0)|^2$ and of the IPR I_2. As explained above, the root weight $|\psi_N(0)|^2$ and of the IPR I_2 are determined by the auxiliary variables $C^{(q)}$ introduced in equation (66). We thus expect that the localized and delocalized phases correspond to the following behavior for the auxiliary variables $C^{(q)}$:

(i) In the localized phase, the auxiliary variables $C^{(q)}$ will remain finite random variables as the number of generations diverge $N \to \infty$. Then the root weight $|\psi_N(0)|^2$ and the IPR I_q remain finite as $N \to \infty$.

(ii) In the delocalized phase, the auxiliary variables $C^{(q)}$ will instead grow exponentially with the number N of generations with some Lyapunov exponents $\lambda_q > 0$ defined by

$$\overline{\ln C^{(q)}} \underset{N\to\infty}{\simeq} \lambda_q N. \tag{81}$$

The corresponding typical behavior of the root weight and of the IPR then reads

$$\overline{\ln |\psi_N(0)|^2} \underset{N\to\infty}{\simeq} -\lambda_1 N \tag{82}$$

and

$$\overline{\ln I_q} \underset{N\to\infty}{\simeq} -(q\lambda_1 - \lambda_q)N. \tag{83}$$

We find numerically that the probability distributions of auxiliary variables $(\ln C^q)$ move as traveling waves of velocity λ_q (see equation (81)) with fixed shape (see figure 12 of appendix B where the fixed shape is shown for $q = 1$ and $q = 2$). We explain in appendix B how the Lyapunov exponents λ_q can be determined via a tail analysis that yields the identity (see equation (B.13))

$$\lambda_q = q\lambda_1 \tag{84}$$

so that the logarithm of the IPR I_q decays slower than linearly in N, because the coefficient in equation (83) exactly vanishes. Physically, one could expect the decay to be of order $(\ln N)$ as in equation (61) concerning pure states on the Cayley tree, but we have not been able to measure the behavior of the IPR, because within the pool method that we use, it turns out that the pool-dependent critical point is not the same for the variables $C^{(1)}$ and for $C^{(2)}$ (see more details in appendix B.3), so that it does not seem easy with the pool method to extract reliable results concerning I_2.

In the remainder of this section, we thus focus on the statistical properties of the root weight $|\psi(0)|^2$ that is determined by the auxiliary variable $C^{(1)}$ via equation (69). The fact that the pool-dependent critical point for $C^{(1)}$ is the same as the critical point found for the Landauer transmission can be understood from the tail analysis of appendices A and B that involve exactly the same integral kernel.

In the delocalized phase, the root weight $|\psi_N(0)|^2$ presents the typical decay of equation (82). We show in figure 9(*a*) that the corresponding Lyapunov exponent $\lambda_1(W)$ vanishes linearly in the critical region

$$\lambda_1(W) \underset{W\to W_c^-}{\simeq} (W_c - W) \tag{85}$$

i.e. we find the same exponent $\nu_{\rm loc} = 1$ as for the divergence of the correlation length of the localized phase (see equation (32)). This can be understood from the tail analysis presented in the Appendices A and B.

We find that the width of the relative variable $z = \ln |\psi_N(0)|^2 - \overline{\ln |\psi_N(0)|^2}$ remains finite in the limit $N \to +\infty$ both in the localized phase and in the delocalized phase: its behavior as a function of the disorder strength W presents a cusp at W_c as shown in figure 9(*b*).

In the localized phase, the root weight remains finite as $N \to \infty$. As shown in figure 10, we measure the following essential singularity:

$$\overline{\ln \psi_\infty(0)} \underset{W\to W_c^+}{\simeq} -\frac{1}{(W - W_c)^{\kappa_0}} \qquad \text{with} \qquad \kappa_0 \simeq 1. \tag{86}$$

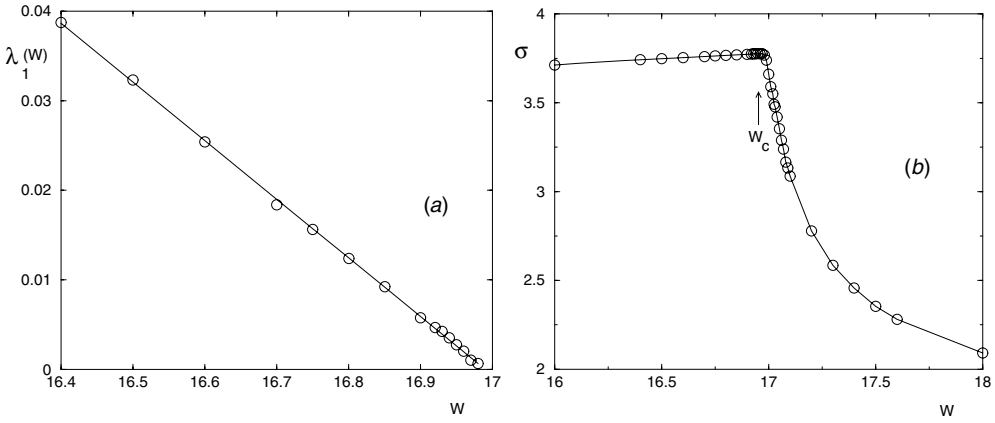

Figure 9. (*a*) In the delocalized phase, the logarithm of the root weight decays linearly $\overline{\ln|\psi_N(0)|^2} \sim -\lambda_1(W)N$: the figure shows that the slope $\lambda_1(W)$ vanishes linearly $\lambda_1(W) \sim (W_c^{\rm pool} - W)$ (see equation (85) with $\nu_{\rm loc} = 1$). (*b*) Width $\sigma = (\overline{z^2})^{1/2}$ of the relative variable $z = \ln|\psi_N(0)|^2 - \overline{\ln|\psi_N(0)|^2}$ in the limit $N \to +\infty$ as a function of the disorder strength W: it remains finite both in the localized and delocalized phases, but it presents a cusp at the critical point W_c.

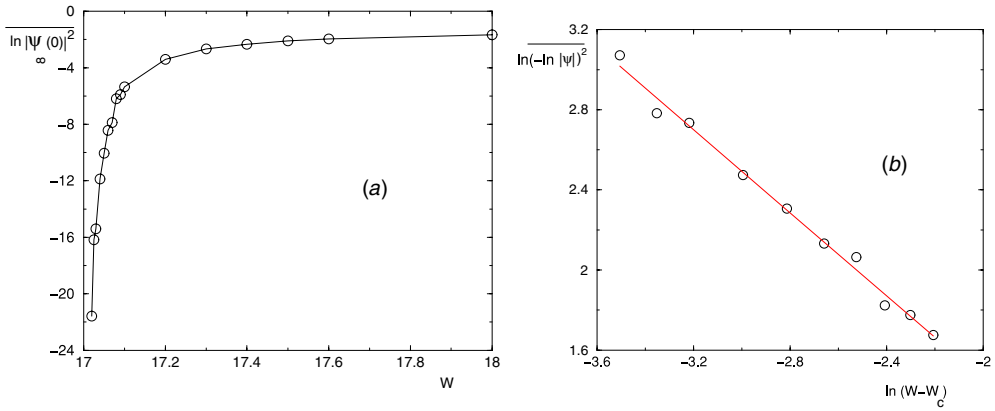

Figure 10. Critical behavior of the root weight $|\psi_\infty(0)|^2$ of an infinite tree in the localized phase: (*a*) $\overline{\ln|\psi_\infty(0)|^2}$ as a function of the disorder strength W and (*b*) $\ln(-\overline{\ln|\psi_\infty(0)|^2})$ as a function of $\ln(W - W_c)$ to measure the exponent of the essential singularity of equation (86): we measure asymptotically a slope of order $\kappa_0 \sim 1$.

As in section 2.3.4, we now discuss the finite-size scaling in the critical region. If there exists some finite-size scaling in the critical region for the typical root weight, the matching of our results in the delocalized phase (see equation (82) and (85)) and in the localized phase (equation (86)) requires a finite-size correlation length exponent $\nu_0^{\rm FS}$ of order

$$\nu_0^{\rm FS} = 1 + \kappa_0 \simeq 2. \tag{87}$$

We have performed the analysis described in section 2.3.4 and we measure that the relaxation length $\xi_{\rm relax}(W)$ toward the finite value of equation (86) diverges with an exponent

$$\xi_{\rm relax}(W) \propto \frac{1}{(W - W_c)^{\nu_{\rm relax}}} \qquad \text{with} \qquad \nu_{\rm relax} \simeq 2 \tag{88}$$

of the order of the exponent $\nu_0^{\rm FS}$ of equation (87). We thus obtain that the critical properties are again qualitatively similar to the critical properties described in [30] (see the summary in appendix C): the traveling phase is characterized by a velocity that vanishes linearly, but the finite size scaling is governed by the relaxation length toward the asymptotic finite value of the non-traveling phase. Exactly at criticality, we thus expect the following stretched exponential decay of the typical transmission:

$$\overline{\ln |\psi_N(0)|^2}|_{W=W_c} \simeq -N^{\rho_0}, \tag{89}$$

where the exponent ρ_0 is related to the other exponents by (see the scaling relations of equations (C.9) and (C.11) in appendix C)

$$\rho_0 = \frac{\kappa_0}{\nu_0^{\rm FS}} = 1 - \frac{1}{\nu_0^{\rm FS}}. \tag{90}$$

From our previous estimate of the exponent $\kappa_0 \simeq 1.$, this corresponds to the numerical value

$$\rho_0 = \frac{\kappa_0}{1+\kappa_0} \simeq 0.5. \tag{91}$$

Again, as explained after equation (42), we have not been able to measure this stretched exponential behavior exactly at criticality from our data, because a precise measure of the exponent ρ_0 would require to be exactly at the critical point.

4. Conclusions and perspectives

In summary, for the Anderson model on the Bethe lattice, we have studied numerically the statistics of the Landauer transmission T_N and the statistics of eigenstates at the center of the band $E = 0$, as a function of the disorder strength W and the number N of generations. We have shown that both the localized phase and the delocalized phase are characterized by the traveling wave propagation of some probability distributions. In the text, we have presented detailed numerical results, and in appendices A and B, we have explained how the velocities of the traveling waves are determined by the tails, via the properties of the integral kernel introduced in [9]. The Anderson transition then corresponds to a traveling/non-traveling critical point for these traveling waves, and the critical properties obtained are very similar to the traveling-wave phase transition studied in [30]: (i) the finite value of the non-traveling phase presents an essential singularity, (ii) the relaxation length toward this essential singularity determines the finite-size scaling in the critical region and (iii) the finite-size correlation length exponent $\nu_{\rm FS}$ is different from the value $\nu_{\rm loc} = 1$ that governs the vanishing of the velocity in the traveling-wave phase. We thus hope that in the future, these properties for Anderson localization on the Cayley tree will be better understood by extending the methods that have been developed recently for the class of the Fisher-KPP traveling waves (see [30, 43] and references therein).

How results obtained on the Bethe lattice are related to properties of Anderson localization in finite dimension d is of course a difficult question. During the history of localization, many values for the upper critical dimension have been proposed such as $d_c = 4, 6, 8, +\infty$. Even within the supersymmetric community, there seems to be different interpretations. Mirlin and Fyodorov [45] consider that the essential singularities that appear on the Bethe lattice, are directly related to the exponential growth of the number of sites with the distance, and will become conventional power-law behavior as soon as $d < \infty$, so that the upper critical dimension is actually $d_c = +\infty$. In contrast, Efetov [15] argues that the results obtained for the Bethe lattice are relevant to Anderson transition in high dimension d when reinterpreted within the so-called 'effective medium approximation'. For the Landauer transmission, the upper

critical dimension d_c can be defined as the dimension where the exponent $\omega(d)$ concerning the width of the sample-to-sample distribution in the localized phase (see equation (2)) vanishes $\omega(d_c) = 0$. This means that for $d \geqslant d_c$, the probability distribution would travel as a traveling wave in the whole localized phase. To determine whether $d_c = +\infty$ or $d_c < +\infty$, it would be thus interesting to understand whether the traveling wave propagation with a fixed shape is possible only on trees or whether it can also occur in sufficiently high dimension d.

In low dimensions, the probability distribution of the logarithm of the transmission is known to broaden with some exponent $\omega(d) > 0$ (see equation (2)) in the localized phase, whereas the probability distribution of the logarithm of IPR is known to shrink with the system size in the delocalized phase [46] (see also figure 4(*a*) of [49] where the same phenomenon occurs for the directed polymer in 1 + 3 dimensions). However traveling wave propagations of the probability distribution $P(\ln I_q)$ of inverse participation ratios I_q have actually been found in finite dimensions but only *exactly at criticality*. This phenomenon has been first obtained for the power-law random band matrix model [47] and has been then observed for the Anderson model in dimensions $d = 3, 4$ [48]: the motions of the typical values $\overline{\ln I_q}$ with $(\ln L)$ determine the multifractal spectrum, whereas the reduced variables $y = I_q / I_q^{\rm typ}$ keep fixed distributions presenting power-law tails with q-dependent exponents. We have actually observed the same behavior for the directed polymer in 1 + 3 dimensions exactly at the localization/delocalization transition (see figures 3(*a*) and (*b*) of [49]). In all these cases, it would be thus very nice to better understand the relations between the tails of the distributions and the motions of the typical values, and to identify the wave equation that underlies these traveling waves.

Finally, our work raises once again the question whether Anderson transitions are characterized by several length scales that diverge with various ν exponents. Here for the Cayley tree, besides the exponent $\nu_{\rm loc} = 1$ that has been predicted for a long time [10], we have found other diverging lengths with the following physical meanings: (i) in the localized phase, besides the exponent $\nu_{\rm loc} = 1$ associated with the divergence of localization length $\xi_{\rm loc} \sim 1/(W - W_c)^{\nu_{\rm loc}=1}$ that describes the far exponential decay of the transmission T (equation (30)), we have found that the critical behavior of the entropy is governed by another diverging length scale with $\nu_s \sim 1.5$ (equation (80)) that characterizes the size where the weight $|\psi(x)|^2$ is concentrated. (ii) In the delocalized phase, we have found that the Landauer transmission reaches its asymptotic value after a length diverging as $\nu_T^{\rm FS} \sim 1.25$ (equation (36)) that governs the finite-size scaling of the transmission in the critical region. Even if the precision of numerically measured critical exponents can always be discussed, we feel nevertheless that our numerical results are not compatible with the existence of the single exponent $\nu_{\rm loc} = 1$. Note that for the directed polymer on the Cayley tree, we have also found previously that the critical properties involve two exponents $\nu = 2$ and $\nu' = 1$ [50]. Whether there exist various exponents ν for the Anderson model in finite dimension d has been debated for a long time. The majority of papers on Anderson localization seem in favor of a single ν (see the reviews [2–7]), but it seems to us that numerical papers actually study always the same type of observables. In particular, we have not been able to find numerical studies concerning the entropy of eigenstates. On the theoretical side, we are not aware of many theories in favor of various ν exponents, except (i) the supersymmetric studies of [14, 15] that involve two different diverging length scales, called respectively the localization length and the phase coherence length. (ii) The pseudo-delocalization transition of the random hopping model in dimension $d = 1$, that is characterized by the two exactly known correlation length exponents $\nu = 1$ and $\nu = 2$ (see [51] and references therein), as in the other models described by the same strong disorder fixed point (see the review [52]). We feel that if localization models exhibit several ν exponents both on the Cayley tree which represents some mean-field $d = \infty$

limit and in some models in dimension $d = 1$, the possibility of various ν for Anderson transition in dimension $d = 3$ should be reconsidered by studying in detail the statistics of various observables.

Appendix A. Tail analysis for the traveling wave of the Landauer transmission in the localized phase

In this appendix, we translate the analysis of [9] concerning the distribution of the self-energy in the localized phase for the traveling-wave propagation of the Landauer transmission discussed in section 2.

The recursion of equation (14) for the complex Riccati variable R_n reads more explicitly in terms of its real and imaginary parts $R_n = X_n - iY_n$ with $X_n \in]-\infty, +\infty[$ and $Y_n \in [0, +\infty[$

$$X_n = -\epsilon_n - \sum_{m=1}^{K} \frac{X_{n-1}(m)}{X_{n-1}^2(m) + Y_{n-1}^2(m)} \tag{A.1}$$

$$Y_n = \sum_{m=1}^{K} \frac{Y_{n-1}(m)}{X_{n-1}^2(m) + Y_{n-1}^2(m)}, \tag{A.2}$$

where the random on-site energies ϵ_n are drawn from the flat distribution of equation (4). The Landauer transmission of equation (26) then reads

$$T_n = 1 - \left| \frac{X_n + i(1 - Y_n)}{-X_n + i(1 + Y_n)} \right|^2 = \frac{4Y_n}{X_n^2 + (Y_n + 1)^2}. \tag{A.3}$$

In the delocalized phase, this recursion of equation (A.2) is difficult to analyze because one has to find the joint distribution of the two finite variables (X, Y) that remain stable upon iteration. In the localized phase however, the problem is simpler [9] as we now recall.

A.1. Linearized recursions in the localized phase

In the localized phase, if the imaginary part Y_n converge toward zero exponentially in n as

$$Y_n = e^{-\nu n} y_n, \tag{A.4}$$

where $\nu > 0$ and where y_n remains a finite random variable upon iteration, one has then to study the simpler recurrence for large n [9, 17]

$$\begin{aligned} X_n &= -\epsilon_n - \sum_{m=1}^{K} \frac{1}{X_{n-1}(m)} \\ e^{-\nu} y_n &= \sum_{m=1}^{K} \frac{y_{n-1}(m)}{X_{n-1}^2(m)}. \end{aligned} \tag{A.5}$$

Note that the form of equation (A.4) corresponds to a traveling wave of velocity ν for the variable $(\ln Y_n)$

$$\ln Y_n = -\nu n + \ln y_n. \tag{A.6}$$

The real part X_n satisfies now a closed recurrence independent of the Y_n, and its stable distribution $P^*(X)$ satisfies the closed equation

$$P^*(X) = \int d\epsilon p(\epsilon) \int dX_1 P^*(X_1) \cdots \int dX_m P^*(X_m) \delta \left[X + \epsilon + \sum_{m=1}^{K} \frac{1}{X_m} \right]. \tag{A.7}$$

An important property of this distribution is that it presents the power-law tail

$$P^*(X) \underset{X\to\pm\infty}{\simeq} \frac{K\,P^*(0)}{X^2} \tag{A.8}$$

because whenever one of the K variables X_i on the right-hand side of equation (A.7) is close to 0, the variable X of the left-hand side is large with $X \sim -1/X_i$.

The stable joint distribution $P^*(X, y)$ satisfies

$$P^*(X,y) = \int \mathrm{d}\epsilon p(\epsilon) \int \mathrm{d}X_1\,\mathrm{d}y_1 P^*(X_1,y_1)\cdots \int \mathrm{d}X_m\,\mathrm{d}y_m P^*(X_m,y_m)\delta \times \left[X+\epsilon+\sum_{m=1}^{K}\frac{1}{X_m}\right]\delta\left[y-\sum_{m=1}^{K}\frac{y_m}{\mathrm{e}^{-v}X_m^2}\right]. \tag{A.9}$$

A.2. Tail analysis

The idea of [9] is to look for the power-law tail in y that is compatible with the recursion equation, i.e. one assumes

$$P^*(X,y) \underset{y\to\infty}{\simeq} \frac{A(X)}{y^{1+\beta}} \tag{A.10}$$

with some exponent $0 < \beta < 1$. Note that, in the traveling wave language of equation (A.6), this is equivalent to look for solutions with an exponential tail $\mathrm{e}^{-\beta u}$ for the variable $u = \ln Y_n + nv = \ln y_n$. So this corresponds to the usual exponential tail analysis of fronts [28, 29], except for the following difference: in usual studies of propagation into unstable phases, it is the 'forward tail' that has an exponential decay and that determines the velocity, whereas in our present case, it is the 'backward tail' that determines the propagation.

In Laplace transform with respect to y, the power-law decay of equation (A.10) corresponds to the following singular expansion near the origin:

$$\begin{aligned}\hat{P}^*(X;s) &\equiv \int_0^{+\infty} \mathrm{d}y\,\mathrm{e}^{-sy}P^*(X,y)\\ &= P^*(X) - \int_0^{+\infty}\mathrm{d}y(1-\mathrm{e}^{-sy})P^*(X,y)\\ &= P^*(X) - \int_0^{+\infty}\frac{\mathrm{d}v}{s}(1-\mathrm{e}^{-v})P^*\left(X,\frac{v}{s}\right)\\ &\underset{s\to 0}{\simeq} P^*(X) - s^\beta A(X)\int_0^{+\infty}\mathrm{d}v\frac{(1-\mathrm{e}^{-v})}{v^{1+\beta}}.\end{aligned} \tag{A.11}$$

Equation (A.9) becomes for the Laplace transform $\hat{P}^*(X;s)$

$$\hat{P}^*(X;s) = \int \mathrm{d}\epsilon p(\epsilon)\int \mathrm{d}X_1\hat{P}^*\left(X_1,\frac{s}{\lambda X_1^2}\right)\cdots\int \mathrm{d}X_m\hat{P}^*\left(X_m,\frac{s}{\lambda X_m^2}\right)\delta\left[X+\epsilon+\sum_{m=1}^{K}\frac{1}{X_m}\right]. \tag{A.12}$$

Using the expansion of equation (A.11), one obtains that the function $A(X)$ has to satisfy the eigenvalue equation

$$\mathrm{e}^{-v\beta}A(X) = K\int\frac{\mathrm{d}X_1}{(X_1^2)^\beta}Q\left(X+\frac{1}{X_1}\right)A(X_1), \tag{A.13}$$

where the function $Q(u)$ represents the stationary distribution of the variable $u = -\epsilon - \sum_{m=2}^{K} \frac{1}{X_m}$

$$Q(u) = \int \mathrm{d}\epsilon p(\epsilon) \int \mathrm{d}X_2 P^*(X_2) \cdots \int \mathrm{d}X_m P^*(X_m) \delta \left[u + \epsilon + \sum_{m=2}^{K} \frac{1}{X_m} \right] \tag{A.14}$$

(see equations (6.5) and (6.6) in [9]).

A.3. Eigenvalue problem for an integral kernel

The tail analysis thus leads to the eigenvalue problem the integral kernel appearing in equation (A.13)

$$\Lambda A(X) = K \int \frac{\mathrm{d}X_1}{\left(X_1^2\right)^{\beta}} Q\left(X + \frac{1}{X_1}\right) A(X_1). \tag{A.15}$$

For each β and W, the integral kernel is positive, and thus one expects some continuous analog of the Perron–Froebenius theorem: the iteration of the integral kernel will converge toward a positive eigenvector $A_0(X)$ that is associated with the maximal eigenvalue $\Lambda_0(\beta, W)$ of the kernel. For instance, for the special case $\beta = 0$, the solution is simply $A(X) = P^*(X)$ (see equations (A.7) and (A.14)) and

$$\Lambda_0(\beta = 0, W) = K. \tag{A.16}$$

Except for this case $\beta = 0$, we are not aware of any explicit solution for the eigenvalue $\Lambda_0(\beta, W)$ (even for the simpler case where the distribution of the on-site energies $p(\epsilon)$ is a Cauchy law and where the distributions $P(X)$ and $Q(u)$ are also Cauchy laws [9, 17]). With equations (A.13) and (A.15), one concludes that at fixed W, each mode β is associated with the velocity $v(\beta, W)$ (equation (A.4))

$$v(\beta, W) = -\frac{1}{\beta} \ln \Lambda_0(\beta, W). \tag{A.17}$$

A.4. Selection of the tail exponent and of the velocity of the traveling wave

The selection of the tail exponent β of equation (A.10) and of the corresponding velocity $v(\beta)$ of equation (A.4) usually depend on the form of the initial condition [26, 28, 29]. In our present case, the initial condition is completely localized (see equation (13))

$$P_{ini}(Y) = \delta(Y - 1). \tag{A.18}$$

In this case, one expects that the solution that will be dynamically selected [26, 28, 29] corresponds to the tail exponent $\beta_{\mathrm{selec}}(W)$ and to the velocity $v_{\mathrm{selec}}(W) = v(\beta_{\mathrm{selec}}(W), W)$ determined by the following extremization:

$$0 = [\partial_\beta v(\beta, W)]_{\beta = \beta_{\mathrm{selec}}(W)} = \left[\frac{1}{\beta^2} \ln \Lambda_0(\beta, W) - \frac{1}{\beta} \frac{\partial_\beta \Lambda_0(\beta, W)}{\Lambda_0(\beta, W)} \right]_{\beta = \beta_{\mathrm{selec}}(w)}. \tag{A.19}$$

The critical point is then determined by the two conditions

$$v(\beta_c, W_c) = 0, \tag{A.20}$$

$$\partial_{\beta_c} v(\beta_c, W_c) = 0. \tag{A.21}$$

A.5. Example in the 'strong disorder approximation'

Since the general discussion is rather obscured by the absence of an explicit expression for the eigenvalue $\Lambda_0(\beta, W)$ of the kernel of equation (A.15), it is useful to consider the following strong disorder approximation (called 'upper limit' condition in [9]), where the recursion for the X_n in equation (A.5) is simply replaced by [9]

$$X_n \simeq \epsilon_n. \tag{A.22}$$

The argument is that in the limit of very large W, the distribution of X has also a width of order W, so that the neglected terms in equation (A.5) are of order K/W. Of course the approximation of equation (A.22) is not very well controlled, because it concerns random variables, and it suppresses important correlations between the variables (X, Y) of equation (A.5). Nevertheless, it is useful to consider it before returning to the true recursions of equation (A.5), because with equation (A.22), the eigenvalue $\Lambda_0(\beta, W)$ is replaced by simple expression [9] (see also section 7.2 of [17] where the approximation of independence between (X, Y) is considered for the Cauchy case)

$$\Lambda_0^{SD}(\beta, W) = K \int \mathrm{d}\epsilon p(\epsilon) |\epsilon|^{-2\beta}. \tag{A.23}$$

The velocity then reads

$$v^{SD}(\beta, W) = -\frac{1}{\beta} \ln \left(K \int \mathrm{d}\epsilon p(\epsilon) |\epsilon|^{-2\beta} \right). \tag{A.24}$$

For the flat distribution $p(\epsilon)$ of random site energies (equation (4)), one thus obtains

$$v^{SD}(\beta, W) = -\frac{1}{\beta} \ln \left(\frac{K}{1-2\beta} \left(\frac{2}{W} \right)^{2\beta} \right) = 2 \ln \frac{W}{2} - \frac{1}{\beta} \ln \left(\frac{K}{1-2\beta} \right). \tag{A.25}$$

The function $v^{SD}(\beta)$ is defined on the interval $0 < \beta < 1/2$: it flows toward $(-\infty)$ in the limits $\beta \to 0$ and $\beta \to 1/2$ with the following behavior:

$$v^{SD}(\beta, W) \underset{\beta \to 0}{\simeq} -\frac{\ln K}{\beta} \tag{A.26}$$

and

$$v^{SD}(\beta, W) \underset{\beta \to 1/2}{\simeq} -\frac{1}{\beta} \ln \frac{1}{1-2\beta}. \tag{A.27}$$

It has a single maximum at $\beta_{\mathrm{selec}}^{SD}$ given by the extremum condition of equation (A.19), so that $\beta_{\mathrm{selec}}^{SD}$ is actually independent of W. For $K = 2$, the selected exponent is of order $\beta_{\mathrm{selec}}^{SD} \simeq 0.3133$ for any W. We note that this value is close to the value $\beta(W = 100) \simeq 0.33$ that we measure for the large disorder $W = 100$ (see figure 5(*a*)). In conclusion, this 'strong disorder approximation' allows us to see explicitly how things work on a simple example, and seems to give a reasonable value of β_{selec} for very large W.

A.6. Argument in favor of $0 < \beta_{\mathrm{selec}}(W) < 1/2$

We now return to the analysis of the full problem of equation (A.5). Here we should say that we do not agree with the discussion of [9] concerning the selection of the tail exponent β:

(i) In [9], the authors conclude that within the localized phase, $\beta_{\mathrm{selec}}(W)$ decreases from unity and reaches $\beta_c = 1/2$ exactly at criticality (see the text between equations (6.8) and (6.9) in [9]).

(ii) In our numerical results of section 2 we have found instead that the selected exponent $\beta_{\rm selec}(W)$ is always smaller than $1/2$: it slightly grows as the disorder strength W decreases and has a value close to 0.5 near criticality (see figure 5(*a*).

We propose the following argument to justify our finding $0 < \beta_{\rm selec}(W) < 1/2$. We think that the tail analysis is actually well defined only on the interval $0 < \beta < 1/2$ for the following reasons. The eigenvalue equation (A.15) relates the behavior of $A(X)$ at $|X| \to \infty$ to the behavior of $A(X)$ near the origin $X \to 0$. For $X \to \infty$, the function $Q\left(X + \frac{1}{X_1}\right)$ will be finite in the region where $\left(X + \frac{1}{X_1}\right)$ is finite, i.e. the integration is dominated by the region $X_1 \sim -1/X$ and we obtain the power-law decay

$$A(X) \underset{|X|\to\infty}{\simeq} \frac{K\,A(0)}{\Lambda_0(\beta)|X|^{2-2\beta}}. \tag{A.28}$$

However the function $A(X)$ has to be integrable at $|X| \to \infty$ to obtain from equation (A.10) the probability of the variable y alone at large y

$$P^*(y) = \int_{-\infty}^{+\infty} {\rm d}X\, P^*(X, y) \underset{y\to\infty}{\simeq} \frac{\int_{-\infty}^{+\infty} {\rm d}X\, A(X)}{y^{1+\beta}}. \tag{A.29}$$

According to equation (A.28), the function $A(X)$ is integrable only for

$$0 < \beta < \tfrac{1}{2} \tag{A.30}$$

i.e. we obtain that the tail analysis has a meaning only for $0 \leqslant \beta < 1/2$. In the limit $\beta \to 0$, we expect from equation (A.16) the same behavior as in equation (A.26)

$$v(\beta, W) \underset{\beta\to 0}{\simeq} -\frac{\ln K}{\beta}. \tag{A.31}$$

Exactly at $\beta = 1/2$, the authors of [9] have argued that

$$[\partial_\beta \Lambda_0(\beta, W)]_{\beta=1/2} = 0 \tag{A.32}$$

for any W, as a consequence of the symmetry $\Lambda_0(\beta, W) = \Lambda_0(1-\beta, W)$ coming from the consideration of the adjoint kernel (see more details around equations (6.7) and (6.8) in [9]). Here in contrast to [9], we think that the region $\beta > 1/2$ is not physical because of equation (A.28), but the condition of equation (A.32) is useful to understand why the critical point determined by equations (A.21) corresponds to the tail exponent [9]

$$\beta(W) \underset{W\to W_{\rm c}^+}{\simeq} \beta_{\rm c} = \tfrac{1}{2}. \tag{A.33}$$

To summarize the selection mechanism, the shape of the velocity $v(\beta, W)$ as a function of the tail exponent β in shown in figure 11 for various disorder strengths W:

(i) In the localized phase $W > W_{\rm c}$, the velocity derivative is negative at $\beta = 1/2$:

$$\begin{aligned}[\partial_\beta v(\beta, W > W_{\rm c})]_{\beta=1/2} &= \left[\frac{1}{\beta^2} \ln \Lambda_0(\beta, W > W_{\rm c})\right]_{\beta=1/2} \\ &= -\left[\frac{1}{\beta} v(\beta, W > W_{\rm c})\right]_{\beta=1/2} < 0.\end{aligned} \tag{A.34}$$

The velocity is extremum at a W-dependent value $\beta_{\rm selec}(W) < 1/2$ and the corresponding selected velocity is positive $v_{\rm selec} > 0$.

(ii) At the critical point $W = W_{\rm c}$, the velocity is extremum at $\beta_{\rm c} = 1/2$ where it vanishes $v_{\rm c} = 0$.

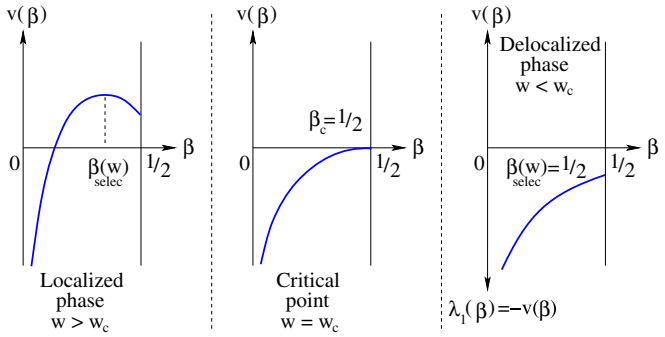

Figure 11. Shape of the velocity $v(\beta, W)$ as a function of the tail exponent β for various disorder strengths W: (i) in the localized phase $W > W_c$, the velocity is extremum at a W-dependent value $\beta_{\rm selec}(W) < 1/2$ and it is positive $v_{\rm selec} > 0$, (ii) at the critical point $W = W_c$, the velocity is extremum at $\beta_c = 1/2$ where it vanishes $v_c = 0$ and (iii) in the delocalized phase, there exists another traveling-wave moving in the other direction of velocity $\lambda_1(\beta, W) = -v(\beta, W) > 0$: this velocity is extremum at $\beta = 1/2$ for any $W < W_c$ (see appendix B for more details).

(iii) In the delocalized phase, the velocity derivative is positive at $\beta = 1/2$:

$$[\partial_\beta v(\beta, W < W_c)]_{\beta=1/2} = \left[\frac{1}{\beta^2} \ln \Lambda_0(\beta, W < W_c)\right]_{\beta=1/2}$$
$$= -\left[\frac{1}{\beta} v(\beta, W < W_c)\right]_{\beta=1/2} > 0. \qquad \text{(A.35)}$$

We explain in appendix B that in this delocalized phase, there exists another traveling-wave moving in the other direction with the velocity $\lambda_1(\beta, W) = -v(\beta, W) > 0$: this velocity $\lambda_1(\beta, W)$ is then extremum at $\beta = 1/2$ for any $W < W_c$ (see appendix B for more details).

As a final remark, we believe that the solution exactly at W_c is not valid anymore because of equation (A.28), and that the appropriate treatment exactly at criticality should replace the finite velocity motion in vn assumed in equation (A.6) by the form

$$\ln Y_n = -(\text{cst}) n^\rho + \ln y_n, \qquad \text{(A.36)}$$

where the anomalous exponent $0 < \rho < 1$ has been discussed in the text (see equations (35) and (42)).

A.7. Conclusion

In conclusion, the analysis of [9] is thus very close to the traveling wave analysis of the directed polymer model [26]: the difference is that in the directed polymer, the variables X_n are random variables independent of the Y_n and the selected $\beta_{\rm selec}$ can be simply obtained from the non-integer moments of X (see section 7.2 in [17]), whereas in the present localization model, the variables X_n and Y_n are correlated and one has thus to solve the eigenvalue problem for the integral kernel of equation (A.15). In the following appendix, we explain how the same ideas can be used in the delocalized phase.

Appendix B. Tail analysis for the traveling waves in the delocalized phase

As explained in section 3, in the delocalized phase, we have considered the recurrence for the real Riccati variable X_n

$$X_n = -\epsilon_n - \sum_{m=1}^{K} \frac{1}{X_{n-1}(m)} \tag{B.1}$$

together with the recurrences of equations (67) for the auxiliary variables $C^{(q)}$ introduced in equation (66).

B. 1. Tail analysis leading to the same integral kernel as in appendix A

To make more visible the similarities with the previous appendix, it is convenient to perform the change of variables

$$D_n^{(q)} \equiv \left(X_n^2\right)^q C_n^{(q)} \tag{B.2}$$

to obtain the following recursions for these variables:

$$D_n^{(q)} = 1 + \sum_{m=1}^{K} \frac{D_{n-1}^{(q)}(m)}{\left(X_{n-1}^2(m)\right)^q}. \tag{B.3}$$

The recursion of equation (B.1) for X_n alone will as before converge to some distribution $P^*(X)$ satisfying equation (A.7). in the delocalized phase, one expects that the variables $C^{(q)}$ will grow exponentially (see equations (81)). We thus set

$$D_n^{(q)} = \mathrm{e}^{n\lambda_q} d^{(q)}, \tag{B.4}$$

where $\lambda_q > 0$ governs the exponential growth and where $d^{(q)}$ remains a finite random variable upon the iteration

$$\mathrm{e}^{\lambda_q} d^{(q)} = \sum_{m=1}^{K} \frac{d^{(q)}(m)}{(X^2(m))^q}. \tag{B.5}$$

The similarity with the discussions of appendix A is now obvious (see equations (A.4) and (A.5)). Assuming the power-law decay

$$P^*(X, d) \underset{d\to\infty}{\simeq} \frac{\Phi(X)}{d^{1+\mu}} \tag{B.6}$$

with $0 < \mu < 1$, one finds that the function $\Phi(X)$ has to satisfy the eigenvalue problem

$$\mathrm{e}^{\mu\lambda_q}\Phi(X) = K \int \frac{\mathrm{d}X_1}{\left(X_1^2\right)^{q\mu}} Q\left(X + \frac{1}{X_1}\right)\Phi(X_1), \tag{B.7}$$

i.e. it is the same integral kernel as in equation (A.13) with the correspondences $\beta \to q\mu$ and $\mathrm{e}^{-v\beta} \to \mathrm{e}^{\mu\lambda_q}$, but now we are interested in the phase $\lambda_q > 0$.

B.2. Selection of tail exponents

We have argued above (see appendix A.6) that the problem for the function $\Phi(X)$ is well defined only for $0 < \beta = q\mu < 1/2$, i.e. the exponent μ_q that governs the power-law of equation (B.6) is restricted to the interval

$$0 < \mu_q < \frac{1}{2q}. \tag{B.8}$$

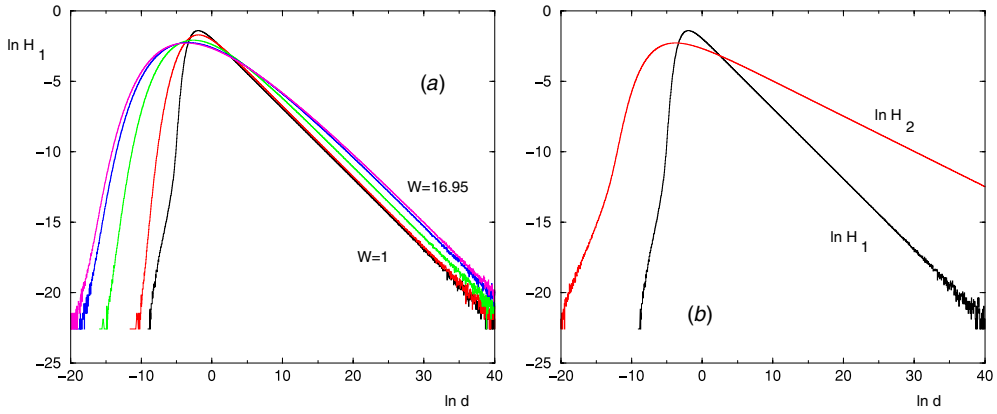

Figure 12. (*a*) Probability distribution H_1 of the variable $\ln d^{(q=1)}$ of equation (B.4) for various disorder strengths $W = 1, 5, 10, 15, 16.95$: the exponent $\mu_1^{\rm selec}$ of equation (B.6) is of order $\mu_1^{\rm selec} \sim 0.5$ in the whole delocalized phase. (*b*) For $W = 1$, comparison of the probability distributions H_1 and H_2 of the variable $\ln d^{(q)}$ for $q = 1$ and $q = 2$: the exponents of equation (B.6) are respectively $\mu_1^{\rm selec} \sim 0.5$ and $\mu_2^{\rm selec} \sim 0.25$ in agreement with equation (B.12).

Denoting as before $\Lambda_0(\beta, W)$ the maximal eigenvalue of the kernel of equation (A.15), each mode μ is associated with the Lyapunov exponent (see equation (A.4))

$$\lambda_q(\mu) = \frac{1}{\mu} \ln \Lambda_0(q\mu, W). \tag{B.9}$$

From equation (A.16), we have the following behavior for $\mu \to 0$:

$$\lambda_q(\mu) \underset{\mu \to 0}{\simeq} \frac{1}{\mu} \ln K \tag{B.10}$$

Near the other boundary $\mu \to 1/(2q)$, the property of equation (A.32) yields that the partial derivative with respect to μ is still negative at $\mu \to 1/(2q)$

$$\left[\partial_\mu \lambda_q(\mu)\right]_{\mu \to 1/(2q)} = \left[-\frac{1}{\mu^2} \ln \Lambda_0(1/2, W)\right]_{\mu \to 1/(2q)} < 0. \tag{B.11}$$

For the special case $q = 1$, the curve $\lambda_1(\beta)$ is directly related via $\lambda_1(\beta) = -v(\beta)$ to the curve $v(\beta)$ discussed in appendix A and shown in figure 11 (see the delocalized case $W < W_{\rm c}$). Since the selected tail exponent $\mu_{\rm selec}$ has to extremize $\lambda_q(\mu)$, we conclude that the selected tail exponents are given by the simple values

$$\mu_q^{\rm selec} = \left(\frac{1}{2q}\right)^- \tag{B.12}$$

in the whole delocalized phase. This is in agreement with our numerical results. We show in figure 12(*a*) the probability distribution of $H_{q=1}(\ln d)$ of the variable $(\ln d)$ of equation (B.4) for various disorder strengths $W = 1, 5, 10, 15, 16.95$: the tail exponent $\mu_1^{\rm selec}$ of equation (B.6) remains of order $\mu_1^{\rm selec} \sim 0.5$. For $q = 2$, we find similarly that the selected tail exponent remains the same within the whole delocalized phase and that it is of order $\mu_2^{\rm selec} \sim 0.25$. In figure 12(*b*), we compare for $W = 1$ the probability distributions $H_{q=1}(\ln d)$ and $H_{q=2}(\ln d)$ of the variables $\ln d^{(q=1)}$: the exponents of equation (B.6) are respectively $\mu_1^{\rm selec} \sim 0.5$ and $\mu_2^{\rm selec} \sim 0.25$.

From equation (B.12), we obtain that the Lyapunov exponents satisfy the identities

$$\lambda_q^{\rm selec} = q\lambda_1^{\rm selec}. \tag{B.13}$$

As explained in the text around equation (84), this identity is important to understand the decay of IPR with the number N of generations in the delocalized phase.

B.3. Finite-size corrections introduced by the pool method

As explained in section 2.3.1, the pool method consists in representing a probability distribution $P(x)$ by a large number $M_{\rm pool}$ of random variables $\{x_i\}$. In particular this introduces a cut-off in the tail of $P(x)$ around $x_{\rm max}$ with $P(x_{\rm max}) \sim 1/M_{\rm pool}$. In the field of traveling waves, the presence of such a cut-off has been much studied (see [43] and references therein): the leading correction to the selected velocity is usually logarithmic in $M_{\rm pool}$

$$v_{\rm selec}(M_{\rm pool}) - v_{\rm selec}(\infty) \sim \frac{J}{(\ln M_{\rm pool})^{\alpha}}. \tag{B.14}$$

For our present problem, where the critical point corresponds to a vanishing velocity $v = 0$, we thus expect that the true critical point $W_{\rm c}(\infty)$ corresponding to $v_{\rm selec}(\infty) = 0$ will be shifted toward a pool-dependent pseudo-critical point $W_{\rm c}(M_{\rm pool})$ corresponding to $v_{\rm selec}(M_{\rm pool}) = 0$. As explained in the text, all the traveling waves encountered in the present paper vanish linearly in $(W - W_{\rm c})$. We thus expect that the difference $[W_{\rm c}(M_{\rm pool}) - W_{\rm c}(\infty)]$ will also decay only logarithmically as $1/(\ln M_{\rm pool})^{\alpha}$. From the analysis presented in appendices A and B, it is obvious that the pool-dependent critical point for the traveling wave of the Landauer transmission (see appendix A) and for the auxiliary variable $C^{(1)}$ or $D^{(1)}$ (see appendix B) are the same because they are defined by the same condition in terms of the eigenvalue $\Lambda_0(\beta)$ of the integral kernel. However, the other variables $C^{(q)}$ or $D^{(q)}$ that have the same true critical point $W_{\rm c}(\infty)$ will not have the same pool-dependent critical point $W_{\rm c}(M_{\rm pool})$, because the constant J in equation (B.14) will depend on q. This is indeed what we observe with our numerical computations with the pool $M_{\rm pool} = 10^5$: the pseudo-critical point $W_{\rm c}(M_{\rm pool})$ for the variable $C^{(2)}$ is below the pseudo-critical point $W_{\rm c}(M_{\rm pool})$ for the variable $C^{(1)}$. We observe that the difference between the two becomes smaller for the bigger pool $M_{\rm pool} = 10^6$. In conclusion, numerical studies based on the pool method are valid for observables that are related to a single traveling wave, but one cannot study the critical properties of observables that depend on two distinct traveling waves that have different pseudo-critical points. This is why in the text, we have not been able to present reliable numerical results for the statistics of IPR I_2 that depends on both $C^{(1)}$ and $C^{(2)}$.

Appendix C. Reminder on the traveling/non-traveling phase transition studied in [30]

In this appendix, we briefly recall the finite-size scaling properties of the traveling/non-traveling phase transition studied in [30], because these properties are useful to interpret our numerical results described in the text.

For a one-dimensional branching random walk in the presence of an absorbing wall moving at a constant velocity v, the survival probability $Q(x,t)$ presents a phase transition at $v = v_c$ with the following critical behavior (see more details in [30]):

(i) For $v < v_c$, it converges exponentially in time toward a finite limit $Q^*(x) > 0$

$$Q(x,t) \simeq Q^*(x) + {\rm e}^{-\frac{t}{\tau}}\phi(x), \tag{C.1}$$

where the limit $Q^*(x)$ presents an essential singularity

$$Q^*(x) \simeq {\rm e}^{-\frac{cte}{(v_{\rm c}-v)^{\kappa}}} \qquad \text{with} \qquad \kappa = \tfrac{1}{2} \tag{C.2}$$

and where the relaxation time τ diverges as

$$\tau \propto \frac{1}{(v_c - v)^{\nu}} \qquad \text{with} \qquad \nu = \frac{3}{2}. \tag{C.3}$$

(ii) For $v > v_c$, it converges exponentially in time toward zero

$$Q(x,t) \simeq e^{-\frac{t}{\tilde{\tau}}}, \tag{C.4}$$

where the relaxation time $\tilde{\tau}$ diverges as

$$\tilde{\tau} \propto \frac{1}{(v_c - v)^{\tilde{\nu}}} \qquad \text{with} \qquad \tilde{\nu} = 1. \tag{C.5}$$

(iii) Exactly at criticality, it converges toward zero with a stretched exponential

$$Q(x,t) \simeq e^{-(cte)t^{\rho}} \qquad \text{with} \qquad \rho = \tfrac{1}{3}. \tag{C.6}$$

(iv) The critical region is described by some finite-size scaling form governed by the relaxation time τ that appears in equation (C.1) (and not by the relaxation time $\tilde{\tau}$ appearing in equation (C.4))

$$\ln Q(x,t) \simeq -t^{\rho} G(t^{1/\nu}(v_c - v)), \tag{C.7}$$

where the scaling function $G(u)$ has the following asymptotic behavior. For $u \to +\infty$, one has the power-law

$$G(u) \underset{u \to +\infty}{\simeq} u^{-\nu\rho} \tag{C.8}$$

to recover the finite limit of equation (C.2) and one has the scaling relation

$$\kappa = \nu\rho. \tag{C.9}$$

For $u \to -\infty$, one has the power-law

$$G(u) \underset{u \to -\infty}{\simeq} (-u)^{\nu(1-\rho)} \tag{C.10}$$

to recover the exponential decay of equation (C.4), and one has the scaling relation

$$\tilde{\nu} = \nu(1 - \rho). \tag{C.11}$$

For the problem considered in [30] all the exponents are exactly known $\tilde{\nu} = 1, \nu = 3/2, \rho = 1/3$ and $\kappa = 1/2$.

In our numerical results presented in the text concerning the traveling/non-traveling phase transitions that occur in Anderson localization on the Bethe lattice, we find very similar critical behavior: the velocity of the traveling wave vanishes linearly with $\tilde{\nu} = 1$, and the finite-size scaling in the critical region is governed by the other exponent ν that appears in the relaxation toward the finite value of the non-traveling phase.

References

[1] Anderson P W 1958 *Phys. Rev.* **109** 1492
[2] Thouless D J 1974 *Phys. Rep.* **13** 93
Thouless D J 1979 *Ill Condensed Matter (Les Houches 1978)* ed R Balian (Amsterdam: North-Holland)
[3] Souillard B 1987 *Chance and Matter (Les Houches 1986)* ed J Souletie (Amsterdam: North-Holland)
[4] Lifshitz I M, Gredeskul S A and Pastur L A *et al* 1988 *Introduction to the Theory of Disordered Systems* (New York: Wiley)
[5] Kramer B and MacKinnon A 1993 *Rep. Prog. Phys.* **56** 1469
[6] Markos P 2006 *Acta Phys. Slovaca* **56** 561
[7] Evers F and Mirlin A D 2008 *Rev. Mod. Phys.* **80** 1355
[8] Abrahams E, Anderson P W, Licciardello D C and Ramakrishnan T V 1979 *Phys. Rev. Lett.* **42** 673

[9] Abou-Chacra R, Anderson P W and Thouless D J 1973 *J. Phys. C: Solid State Phys.* **6** 1734
See also Abou-Chacra R and Thouless D J 1974 *J. Phys. C: Solid State Phys.* **7** 65
[10] Kunz H and Souillard B 1983 *J. Phys. Lett.* **44** L411
[11] Mirlin A D and Fyodorov Y V 1991 *Nucl. Phys.* B **366** 507
[12] Zirnbauer M R 1986 *Phys. Rev.* B **34** 6394
[13] Verbaarschot J J M 1988 *Nucl. Phys.* B **300** 263
[14] Efetov K B and Viehweger O 1992 *Phys. Rev.* B **45** 11546
[15] Efetov K B 1997 *Supersymmetry in Disorder and Chaos* (Cambridge: Cambridge University Press)
[16] Derrida B and Rodgers G J 1993 *J. Phys. A: Math. Gen.* **26** L457
[17] Miller J D and Derrida B 1994 *J. Stat. Phys.* **75** 357
[18] Shapiro B 1983 *Phys. Rev. Lett.* **50** 747
[19] Chalker J T and Siak S 1990 *J. Phys.: Condens. Matt.* **2** 2671
[20] Bell P M and MacKinnon A 1994 *J. Phys.: Condens. Matt.* **6** 5423
[21] Basko D M, Aleiner I L and Altshuler B L 2006 *Ann. Phys.* **321** 1126
Basko D M, Aleiner I L and Altshuler B L 2007 *Phys. Rev.* B **76** 052203
[22] Altshuler B L, Gefen Y, Kamenev A and Levitov L S 1997 *Phys. Rev. Lett.* **78** 2803
[23] Silvestrov P G 2001 *Phys. Rev.* B **64** 113309
[24] Gornyi I V, Mirlin A D and Polyakov D G 2005 *Phys. Rev. Lett.* **95** 206603
[25] Oganesyan V and Huse D A 2007 *Phys. Rev.* B **75** 155111
[26] Derrida B and Spohn H 1988 *J. Stat. Phys.* **51** 817
[27] Majumdar S N and Krapivsky P L 2000 *Phys. Rev.* E **62** 7735
Majumdar S N and Krapivsky P L 2002 *Phys. Rev.* E **65** 036127
Majumdar S N and Krapivsky P L 2003 *Physica* A **318** 161
Majumdar S N 2003 *Phys. Rev.* E **68** 026103
[28] Ebert U and Saarloos W van 2000 *Physica* D **146** 1
Saarloos W van 2003 *Phys. Rep.* **386** 29
[29] Brunet E 2007 Research lecture on the stochastic Fisher-KPP front equation (Marseille 2007) (available at http://www.lps.ens.fr/ebrunet/)
[30] Derrida B and Simon D 2007 *Europhys. Lett.* **78** 60006
Simon D and Derrida B 2008 *J. Stat. Phys.* **131** 203
Simon D 2008 *PhD Thesis* (available at http://tel.archives-ouvertes.fr/tel-00286612/fr/)
[31] Landauer R 1970 *Philos. Mag.* **21** 863
[32] Anderson P W, Thouless D J, Abrahams E and Fisher D S 1980 *Phys. Rev.* B **22** 3519
[33] Anderson P W and Lee P A 1980 *Suppl. Prog. Theor. Phys.* **69** 212
[34] Luck J M 1992 Systèmes désordonnés unidimensionnels, Collection Alea Saclay Series (Cambridge: Cambridge University Press)
[35] Stone A D and Szafer A 1988 *IBM J. Res. Dev.* **32** 384
[36] Prior J, Somoza A M and Ortuno M 2005 *Phys. Rev.* B **72** 024206
Somoza A M, Prior J and Ortuno M 2006 *Phys. Rev.* B **73** 184201
Somoza A M, Ortuno M and Prior J 2007 *Phys. Rev. Lett.* **99** 116602
[37] Sade M and Berkovits R 2003 *Phys. Rev.* B **68** 193102
[38] Banavar J R and Bray A J 1987 *Phys. Rev.* B **35** 8888
Nifle M and Hilhorst H J 1992 *Phys. Rev. Lett.* **68** 2992
Aspelmeier T, Bray A J and Moore M A 2002 *Phys. Rev. Lett.* **89** 197202
[39] Cook J and Derrida B 1989 *J. Stat. Phys.* **57** 89
[40] Monthus C and Garel T 2008 *Phys. Rev.* E **77** 021132
Monthus C and Garel T 2008 *Phys. Rev.* B **77** 134416
[41] Klein A 1996 *Commun. Math. Phys.* **177** 755
[42] Monthus C and Texier C 1996 *J. Phys. A: Math. Gen.* **29** 2399
[43] Brunet E and Derrida B 1997 *Phys. Rev.* E **56** 2597
Brunet E and Derrida B 2001 *J. Stat. Phys.* **103** 269
Brunet E and Derrida B 2004 *Phys. Rev.* E **70** 016106
Brunet E, Derrida B, Mueller A H and Munier S 2006 *Europhys. Lett.* **76** 1
Brunet E, Derrida B, Mueller A H and Munier S 2006 *Phys. Rev.* E **73** 056126
Brunet E, Derrida B, Mueller A H and Munier S 2007 *Phys. Rev.* E **76** 041104
[44] Mirlin A D and Fyodorov Y V 1997 *Phys. Rev.* B **56** 13393
[45] Mirlin A D and Fyodorov Y V 1994 *Phys. Rev. Lett.* **72** 526
Mirlin A D and Fyodorov Y V 1994 *J. Physique I (France)* **4** 655

[46] Brndiar J and Markos P 2008 *Phys. Rev.* B **77** 115131
[47] Evers F and Mirlin A D 2000 *Phys. Rev. Lett.* **84** 3690
Mirlin A D and Evers F 2000 *Phys. Rev.* B **62** 7920
[48] Mildenberger A, Evers F and Mirlin A D 2002 *Phys. Rev.* B **66** 033109
[49] Monthus C and Garel T 2007 *Phys. Rev.* E **75** 051122
[50] Monthus C and Garel T 2007 *Phys. Rev.* E **75** 051119
[51] McKenzie R H 1996 *Phys. Rev. Lett.* **77** 4804
Balents L and Fisher M P A 1997 *Phys. Rev.* B **56** 12970
[52] Igloi F and Monthus C 2005 *Phys. Rep.* **412** 277